PERGAMON

International Journal of Solids and Structures 36 (1999) 1–34

INTERNATIONAL JOURNAL OF SOLIDS and STRUCTURES

Stable crack growth along a brittle/ductile interface—II. Small scale yielding solutions and interfacial toughness predictions

K. Bose[a,*,1], P. A. Mataga[b], P. Ponte Castañeda[c]

[a]*Mechanical Engineering and Applied Mechanics, University of Pennsylvania, Philadelphia, PA 19104, U.S.A.*
[b]*Bell Laboratories, 1HC 1U-330, Naperville, IL 60566, U.S.A.*
[c]*Mechanical Engineering and Applied Mechanics, University of Pennsylvania, Philadelphia, PA 19104, U.S.A.*

Received 8 October 1996; in revised form 23 August 1997

Abstract

The problem of a crack growing steadily and quasi-statically along a brittle/ductile interface under plane strain, mixed mode, and small scale yielding conditions is considered. The ductile material is assumed to be characterized by the J_2-flow theory of plasticity with linear strain hardening, while the brittle material is assumed to be linear elastic. A displacement-based finite element method, exploiting the convective nature of the problem, is utilized to solve the relevant boundary value problem. In Part I of this work, the corresponding asymptotic problem was solved. This paper addresses the full-field problem in order to validate the asymptotic solutions, and to explore the physical implications of the results. The numerical full-field results are found to be in good agreement with the analytical asymptotic solutions. In particular, the full-field results strongly suggest that the stress fields in the vicinity of the crack tip are variable-separable of the power singular type; and also that the mode mix of the near-tip stress fields is, to a large extent, independent of the applied elastic mode mix. The amplitude (the plastic stress intensity factor) and the regions of validity of the asymptotic fields are estimated from the full-field results, and are observed to be strongly dependent on the applied mode mix. The remote elastic loading fields appear to influence the near-tip fields, primarily, through the plastic stress intensity factor. The present work also explores the suggestion made by Bose and Ponte Castañeda (1992) that the solutions to the small scale yielding problem may be used in the context of a standard crack growth criterion, requiring that continued growth take place with a fixed near-tip crack opening profile, to obtain theoretical predictions for the dependence of interfacial toughness on the applied mode mix. Based on the numerical results, predictions for mixed mode toughness of the brittle/ductile interface are reported. The results, which are in qualitative agreement with available experimental data and also with some recent theoretical results, predict a strong dependence of interfacial toughness on mode mix. This suggests that ductility provides the main operating mechanism for explaining the dependence of interfacial toughness on the mode mix of the applied loading fields, during steady crack growth.

* Corresponding author.
[1] Presently at Hibbitt, Karlsson and Sorensen, Inc., 1080 Main Street, Pawtucket, RI 02860, U.S.A.

0020–7683/99/$—see front matter
PII: S0020–7683(97)00270–9

1. Introduction

It is well known that crack growth under mixed mode conditions is often observed in practice due to a number of reasons, including asymmetry of the cracked specimen in the applied loading with respect to the crack orientation, and inhomogeneity in the material. Potential applications of this phenomenon range from the microscopic, as in crack growth along grain boundaries, to the macroscopic, as in delamination of composite materials and decohesion of coatings and thin films. A particular case of mixed mode fracture is one where the crack propagates along the interface between two dissimilar materials, with at least one of the materials having appreciable ductility. It has been observed experimentally (Trantina, 1972; Anderson et al., 1974; more recently, Liechti and Hanson, 1988; Cao and Evans, 1989; Wang and Suo, 1990; Liechti and Chai, 1991, 1992; see Hutchinson and Suo, 1991, for an extensive literature survey on this subject) that the interfacial toughness for initiation and for crack growth is a strong function of the mode mix of the applied loading fields, with the near mode II toughness being at times a factor of five times or even higher than the near mode I toughness. Experimental work by Anderson et al. (1974) suggested that roughness of the fracture surface due to microbranching of the main crack into the more brittle phase may have contributed to the increase in overall toughness with increasing shear. Evans and Hutchinson (1989) proposed a model which accounted for mixed mode interfacial toughness through asperity interaction behind the crack tip, for cracks along the interface between two brittle materials. Liechti and Chai (1992) measured the toughness of a glass/epoxy interface over a wide range of mode mixes, and carried out finite element analysis to study the near-front behavior during crack initiation. The authors considered plastic and bulk viscoelastic dissipation along with asperity interaction to account for the experimentally measured dependence of toughness on mode mix. Based on the results, they argued that even the combined effects of dissipation and asperity interaction may not account for the dependence of interfacial toughness on mode mix when one of the two materials is sufficiently ductile. They noted that the inelastic deformation of the epoxy phase merited further consideration. Recently, Bose and Ponte Castañeda (1992, henceforth referred to as BPC), and Tvergaard and Hutchinson (1993, henceforth referred to as TH) have independently proposed theoretical models to account for the strong dependence of interfacial toughness on mode mix. While the models proposed by the above authors (BPC vs TH) differ in their details, they both conclude that plasticity may be playing an important role in determining interfacial toughness as a function of mode mix. Both these models will be discussed in some detail in the rest of the paper.

In Part I of this work (Ponte Castañeda and Mataga, 1991—henceforth referred to as PCM), the near-tip asymptotic problem of a crack growing steadily and quasi-statically along a brittle/ductile interface was solved. The authors considered both plane strain and anti-plane strain crack growth. For crack growth under plane strain conditions, it was shown that only four types of variable-separable solutions are possible in the vicinity of the propagating crack tip. Two of these four solutions are of the tensile/compressive type with the stress fields being predominantly either tensile or compressive in nature in the line ahead of the crack, while the other two solutions are of the shear type with predominantly either positive or negative shear stress fields in the line ahead of the crack. In general, no other intermediate solutions were found. The results of the above work suggest that, to a large extent, the mode mix of the near-tip fields may be independent of the mode mix of the applied loading fields, and also that, the effect of the far-field is felt at the crack tip

primarily through the plastic stress intensity factor. The above results are somewhat unexpected, given the well-known corresponding results for stationary cracks in homogeneous materials (Shih, 1974); where the near-tip mode mix depends on the far-field mode mix and varies continuously with it. Subsequently, BPC extended the work of PCM to the problem of steady quasi-static crack growth along the interface between two generally dissimilar elastoplastic solids. The main results of the latter work generalize those reported by PCM. In addition to the asymptotic results, some preliminary finite element results of the corresponding full-field problem were also reported by BPC. The full-field results appeared to be consistent with the predictions of the asymptotic analysis, and indicated that for a wide range of remote loading fields, the near-tip stress state is either the tensile or the compressive state predicted by the asymptotic analysis. Based on the asymptotic and full-field results, the authors explored possible physical implications of the discrete near-tip mode mix phenomenon. A ductile mechanism to explain the experimentally observed dependence of interfacial toughness on mode mix was proposed.

Bose and Ponte Castañeda (1995) further developed the ductile mechanism proposed by BPC. By making use of the near-tip results that were obtained in earlier work, the authors constructed approximate full-field solutions to the plane strain small scale yielding problem of steady quasi-static crack growth along a brittle/ductile interface. These approximate solutions satisfied the criteria that they asymptotically approach the near-tip tensile fields close to the crack tip, and the well-known mixed mode elastic singular fields in the far-field. The solutions involved certain degrees of freedom (the plastic stress intensity factor being one of them) which were optimized through the application of a variational statement of compatibility for a sequence of small scale yielding problems with different values of the applied mode mix. The full-field solutions were subsequently used in the context of a standard crack growth criterion, requiring that continued growth take place with a constant crack opening profile, to obtain theoretical predictions for the dependence of interfacial toughness on mode mix. The results, which were in qualitative agreement with available experimental data (Cao and Evans, 1989; Liechti and Chai, 1992; and others), and also with the theoretical results by TH, predicted a strong dependence of toughness on mode mix, and also on material properties, particularly, on the hardening parameter. Although the above work helped in isolating a physical mechanism that is responsible for the strong dependence of interfacial toughness on mode mix, it depended on the availability of the asymptotic solutions, and did not directly address the issue of the validity of the asymptotic solutions themselves.

Thus, while asymptotic analyses of the above kind are important, they need to be verified by full-field numerical studies. The plastic stress intensity factor needs to be determined from the numerical results. Also, the asymptotic results do not provide any information on the region of validity of the near-tip fields. The region of validity is important in order to assess the physical relevance of the near-tip fields. The latter fields can be expected to be significant physically only if their regions of validity are bigger than the fracture process zone, which is typically estimated to be a small fraction of the size of the plastic zone at the crack tip. The above observations regarding the necessity of a full-field analysis are generally true for any problem involving an analysis of crack-tip fields, where the governing equations admit an asymptotic solution without having to consider the details of remote loading conditions and/or geometry of the cracked specimen. The asymptotic analysis of the mixed mode crack growth problem, however, leaves some more unanswered questions. Most significantly, it does not predict the conditions under which one of the (only) four near-tip states would be preferred over the other three. Full-field numerical studies

have recently been carried out by Omprakash and Narasimhan (1996) for anti-plane strain quasi-static crack growth along a brittle/ductile interface, and by Ranjith and Narasimhan (1996) for anti-plane strain dynamic crack growth at a brittle/ductile interface. The near-tip solutions obtained by Omprakash and Narasimhan agree very well with the asymptotic anti-plane strain solutions reported in PCM. The authors also studied the range of dominance of the asymptotic fields of PCM as a function of the material parameters, and concluded that as long as the material strain-hardens sufficiently, the asymptotic fields have significant ranges of validity.

To address the issues discussed in the last paragraph, in the present work the small scale yielding problem for plane strain crack growth under mixed mode conditions is solved numerically using the finite element method. The primary aim of this work is to verify the extent to which the conclusions that were deduced at the asymptotic level are true as one moves "sufficiently" close to the growing crack tip. The issue of identifying the remote conditions that trigger one near-tip state as opposed to the others is explored in some detail. To this end, solutions to the small scale yielding problem are obtained for a wide range of remote loading fields with different mode mixes. Subsequently, by noting the near-tip state (in particular, the near-tip mode mix) for a given remote condition, connections are made among the wide range of possible remote loading fields and their associated near-tip states. Based on the numerical results, the relevance of the ductile mechanism (BPC) to explain the experimentally observed dependence of interfacial toughness on the mode mix of the remote loading fields is further explored. The numerical results for interfacial toughness vs mode mix reported here based on the full-field finite element results to the small scale yielding problem are in qualitative agreement with experimental (Cao and Evans, 1989; Liechti and Chai, 1992; and others), as well as available theoretical results (TH, Bose and Ponte Castañeda, 1995).

The plan of the paper is as follows. In the next section, the small scale yielding boundary value problem is outlined, and the finite element method utilized to solve the problem is briefly discussed. In Section 3, numerical results for the small scale yielding problem are presented. Connections are also made between the numerical results and the analytic asymptotic fields reported earlier by PCM. It is observed that the asymptotic fields may have significant regions of validity; so that their use in making global predictions can be justified. Finally in Section 4, the ductile mechanism that addresses the well-known dependence of interfacial toughness on mode mix is presented, and the predictions based on the mechanism are discussed and compared against available experimental and theoretical results.

2. Formulation

Figure 1(a) depicts a plane strain crack propagating steadily and quasi-statically along the interface between generally dissimilar materials, under small scale yielding and mixed mode conditions. The uniaxial constitutive response (Fig. 1(b)) of each material is assumed to be characterized by J_2-flow theory of plasticity, with linear strain hardening. The pertinent material parameters are, for each material; the hardening parameter $\alpha^{(r)}$, which is the ratio of the (constant) tangent modulus in tension $E_t^{(r)}$ to the Young's modulus $E^{(r)}$; the Poisson's ratio, $\nu^{(r)}$; and the yield stress in shear, $\tau_0^{(r)}$. Here, the superscript in parenthesis ($r = 1, 2$) refers to the materials in the lower, and upper halves, respectively.

Let x_i ($i = 1, 2, 3$) be a Cartesian coordinate system of fixed orientation traveling with the crack

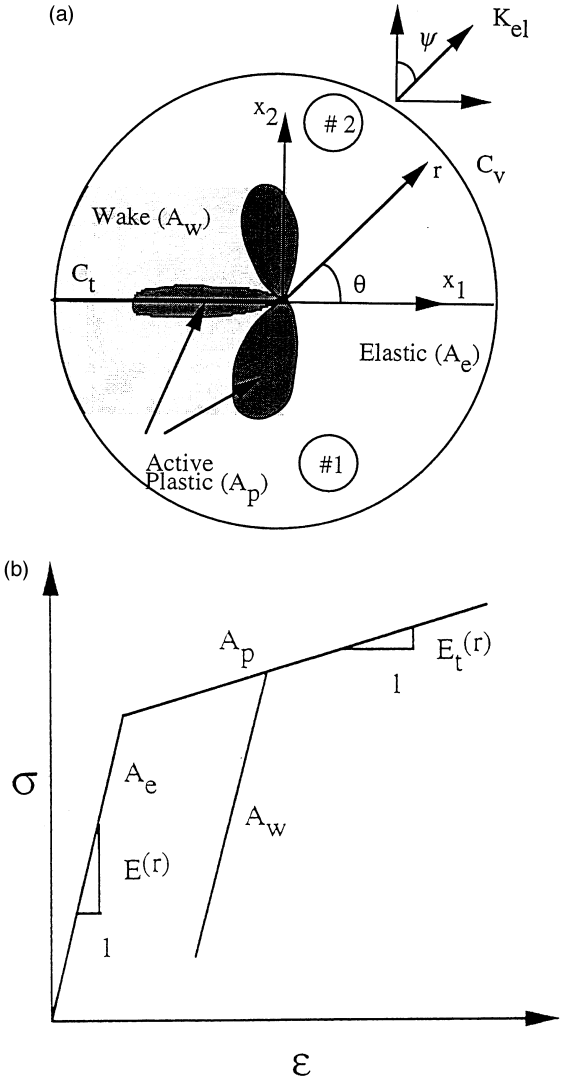

Fig. 1. (a) Steady-state crack growth under small scale yielding conditions. (b) Uniaxial stress–strain relation for a ductile material that deforms according to the J_2-flow theory of plasticity with linear strain hardening.

tip such that the x_3-axis lies along the crack edge as shown in Fig. 1(a). Also, let r, θ be polar coordinates in the x_1–x_2 plane, with $\theta = 0$ coinciding with the positive x_1 direction. The crack tip is assumed to move with velocity $\mathbf{V} = V\mathbf{e}_1$ with respect to the stationary coordinate system X_i. It is assumed that the crack has reached steady state so that the crack tip speed V is constant; then the material derivative of any field quantity A is given by

$$\dot{A} = -VA_{,1} \tag{1}$$

The comma denotes differentiation with respect to x_1.

The dependent variables of the problem are the in-plane stress components $\sigma_{\alpha\beta}$ ($\alpha, \beta = 1, 2$), the out-of-plane normal stress component σ_{33}, and the in-plane velocities v_α. Alternatively, the above variables may be expressed in terms of the cylindrical components of the stress tensor $\boldsymbol{\sigma}$, and the velocity vector $\mathbf{v}$. Under the plane strain assumption, these variables are functions of the in-plane coordinates x_α only.

Under the assumption of quasi-static growth, the governing equations are the equilibrium equations:

$$(r\sigma_{rr})_{,r} + \sigma_{r\theta,\theta} - \sigma_{\theta\theta} = 0 \tag{2}$$

$$(r\sigma_{r\theta})_{,r} + \sigma_{\theta\theta,\theta} + \sigma_{r\theta} = 0 \tag{3}$$

and the constitutive equations for the two ductile solids with bilinear uniaxial stress–strain relations:

$$\mathbf{D} = (1/E^{(r)})[(1+v^{(r)})\Sigma - v^{(r)} Tr(\Sigma)\mathbf{I} + \dot{\Lambda}^{(r)}\mathbf{S}] \tag{4}$$

where

$$\dot{\Lambda}^{(r)} = (3/2)((\underline{\alpha}^{(r)})^{-1} - 1)(\dot{\sigma}_e/\sigma_e). \tag{5}$$

In the above equations, $\mathbf{D} = (1/2)[\nabla\mathbf{v} + (\nabla\mathbf{v})^T]$ is the rate-of-deformation tensor, $\Sigma = \dot{\boldsymbol{\sigma}}$ is the stress-rate tensor, $\mathbf{S} = \boldsymbol{\sigma} - (1/3)Tr(\boldsymbol{\sigma})\mathbf{I}$ is the stress-deviator tensor, $\sigma_e = [(3/2)\mathbf{S}:\mathbf{S}]^{1/2}$ is the effective stress, $\mathbf{I}$ is the second-order identity tensor, and $\underline{\alpha}^{(r)}$ is either $\alpha^{(r)}$ or unity depending on whether a given material particle is in a plastic loading or elastic unloading region. The latter distinction is made due to the singular nature of the stress fields close to the propagating crack tip. Thus, earlier work (Dean and Hutchinson, 1981, more recently, Varias and Shih, 1993, TH, and others) have demonstrated that there is a plastic loading region directly ahead of the crack tip which is due to initial plastic loading of material particles as the crack tip approaches them. This is followed by an elastic unloading, wake region, containing plastically deformed material, which sometimes encloses a small region of further plastic reloading adjacent to the crack flanks. These active (A_p; see Fig. 1(a)) and inactive (A_w) plastic regions are in turn surrounded by a large elastic region ($A_e = A - A_p - A_w$), which is driven on its remote ($r \to \infty$) boundary C_v by the mixed mode elastic singular tractions, given by

$$T_\alpha = \sigma^\infty_{\alpha\beta} n_\beta \tag{6}$$

where $\boldsymbol{\sigma}^\infty$ is the stress field associated with the mixed-mode elastic singular fields, and $\mathbf{n}$ is the outer normal to C_v. The elastic singular stress fields (Williams, 1959) are given by:

$$\sigma^\infty_{\alpha\beta}(r,\theta) = \mathrm{Re}\,[Kr^{i\varepsilon}](2\pi r)^{-1/2}\tilde{\sigma}^{\mathrm{I}}_{\alpha\beta}(\theta,\varepsilon) + \mathrm{Im}\,[Kr^{i\varepsilon}](2\pi r)^{-1/2}\tilde{\sigma}^{\mathrm{II}}_{\alpha\beta}(\theta,\varepsilon) \tag{7}$$

where K is the complex elastic stress intensity factor, $i = \sqrt{-1}$, r and θ are as depicted in Fig. 1(a), Re and Im stand for real and imaginary parts, respectively, of a complex number, $\tilde{\sigma}^{\mathrm{I}}_{\alpha\beta}$ and $\tilde{\sigma}^{\mathrm{II}}_{\alpha\beta}$ are the mode I and mode II angular variations of the stress components, and ε is the elastic bimaterial parameter, defined by

$$\varepsilon = (1/2\pi)\ln[((3-4v^{(1)})/\mu^{(1)} + 1/\mu^{(2)})/((3-4v^{(2)})/\mu^{(2)} + 1/\mu^{(1)})]. \tag{8}$$

where $v^{(r)}$ and $\mu^{(r)}$ are the Poisson's ratio and shear modulus, respectively, of the r-th phase ($r = 1, 2$). The mixed mode elastic singular stress fields can be fully characterized in terms of the

magnitude of the complex stress intensity factor K_{el} ($=|K|$), and a length-scale (L) dependent measure of phase angle ψ, given by:

$$\psi = \tan^{-1}(\mathrm{Im}(KL^{i\varepsilon})/\mathrm{Re}(KL^{i\varepsilon})). \tag{9}$$

The choice of L is arbitrary, and the specific value used in this work will be given later. When $\varepsilon = 0$, (9) reduces to:

$$\psi = \tan^{-1}(K_{\mathrm{II}}/K_{\mathrm{I}}) \tag{10}$$

where K_{II} and K_{I} are the conventional mode II, and mode I stress intensity factors, respectively. Definitions (9) and (10) imply that $\psi = 0^\circ$ for applied tension, while $\psi = \pm 90^\circ$ for applied positive/negative shear. While there is no difference between positive and negative applied shear for a crack in a homogeneous material, lack of symmetry for an interfacial crack requires that such a distinction be made. Thus, for a crack along the interface between a ductile material and a rigid substrate, it may be expected that positive shear would lead to opening of the crack, while negative shear would lead to crack closure.

The statement of the small scale yielding boundary problem is completed by specifying that the crack faces are traction free. Thus, on C_t,

$$T_\alpha = 0. \tag{11}$$

2.1. *Summary of the finite element method*

The governing eqns (2)–(4) along with the boundary conditions (6) and (11) are solved using the finite element method. The finite element formulation follows that of Dean and Hutchinson (1981), with further modifications by Mataga (1986, 1989) to accommodate dissimilar material properties. The reader is referred to the above references (see also Varias and Shih, 1993) for a detailed description of the formulation, which is displacement based, and utilizes a variational statement of equilibrium and the steady-state nature of the problem to solve for the plastic strains in an iterative manner. The domain A in Fig. 1(a) is meshed with constant strain triangles. The building block of the mesh is the quadrilateral (which is made up of four triangles). The smallest element, which sits in the fine-meshed near-tip region is 10^{-4} times a typical measure of the plastic zone size, which for small scale yielding is given by:

$$r_p = (K_{el}/\tau_0^{(2)})^2/2\pi. \tag{12}$$

The small scale yielding condition is approximated by applying the elastic singular fields (6) as boundary conditions on C_v, which is at a distance of approximately $10r_p$ from the crack tip. As pointed out earlier, the elastic fields are characterized by the magnitude of the elastic stress intensity factor K_{el}, and a length (L) dependent measure of mode-mix ψ. Following TH, the choice $L = r_p$ is made in this work. By making the above choice for L, the mode mix is described in terms of physically meaningful quantities (roughly, an estimate of the mode mix at the plastic boundary if plasticity effects on the stress state were negligible), and is independent of artificial aspects such as the units of length L.

For the purpose of presenting the results, only one material pair is considered, and the small scale yielding problem is solved for a series of values of ψ; the latter varying incrementally

from pure positive shear ($\psi = 90^\circ$) to pure negative shear ($\psi = -90^\circ$), and includes different intermediate combinations of tension and shear. The upper half plane is assumed to be ductile with $\alpha^{(2)} = 0.01$ and $\tau_0^{(2)} = 0.01$, while the lower half is assumed to be elastic ($\alpha^{(1)} = 1$). The ratio of the Young's moduli of the halves $\beta = E^{(2)}/E^{(1)}$ is chosen to be 0.01 in order to approximate a ductile solid bonded over a rigid substrate. The Poisson's ratios of the halves are chosen to be $\nu^{(1)} = \nu^{(2)} = 0.495$ in order to approximate incompressible phases. The latter approximation leads to the simplifying feature that the elastic mismatch $\varepsilon \approx 0$, so that the elastic interfacial fields are nearly non-oscillatory. The remote loads are such that $r_p = 1$. The small scale yielding results are expected to depend upon material properties also. However, such a dependence is not explored in the present work.

Note that, because the small scale yielding problem considers a semi-infinite crack in an infinite medium, there is no length scale in the formulation other than that introduced by the plastic zone size r_p. The unit of r_p depends on the choice of units for the elastic stress intensity factor, K_{el}, and that for the yield stress of the ductile material, $\tau_0^{(2)}$. No specific choice of units has been made in the presentation of the results. Instead, a consistent choice of units is assumed.

2.2. *Near-tip singular fields and mode mix*

As asymptotic analysis of the problem (PCM, BPC) led to variable-separable (in r and θ) stress and velocity fields in the vicinity of the propagating crack tip. The near-tip ($r \to 0$) stresses are of the form:

$$\sigma_{ij}^0(r,\theta) = K_{pl}(2\pi r)^s \tilde{\sigma}_{ij}^0(\theta), \tag{13}$$

and the near-tip velocities are of the form:

$$v_\alpha^0(r,\theta) = K_{pl}(V/E^{(2)})((2\pi r)^s/s)\tilde{v}_\alpha^0(\theta). \tag{14}$$

In eqns (13) and (14), s is the strength of the singularity of the near-tip fields, $E^{(2)}$ is the Young's modulus of the ductile material, $\tilde{\sigma}_{ij}^0(\theta)$ and $\tilde{v}_\alpha^0(\theta)$ are angular variations of the stress, and velocity fields, respectively, and K_{pl} is the plastic stress intensity factor. While the quantities, s, $\tilde{\sigma}_{ij}^0(\theta)$ and $\tilde{v}_\alpha^0(\theta)$ are determined by the asymptotic analysis, K_{pl} remains undetermined from an asymptotic analysis alone, and its determination requires the solution of the small scale yielding problem. For a given material pair, the authors found only four asymptotic solutions of the form (13) and (14). Two of these four solutions are of the "tensile/compressive" type, with the stress field being predominantly either tensile or compressive in nature in the line ahead of the crack; while the other two solutions are of the "shear" type, with predominantly either positive or negative shear stress field in the line ahead of the crack.

In order to describe the characteristics of the near-tip fields more precisely, it is useful to introduce the following "mode-mix" functions:

$$m(r) = (2/\pi)\tan^{-1}(\sigma_{\theta\theta}(r,\theta = 0^\circ)/\sigma_{r\theta}(r,\theta = 0^\circ)), \tag{15}$$

$$n(r) = (2/\pi)\tan^{-1}(\sigma_{r\theta}(r,\theta = 90^\circ)/\sigma_{\theta\theta}(r,\theta = 90^\circ)), \tag{16}$$

$$l(r) = (2/\pi)\tan^{-1}(v_y(r,\theta = 180^\circ)/v_x(r,\theta = 180^\circ)). \tag{17}$$

Owing to the properties of the inverse trigonometric function, the mode-mix functions are periodic with a period of four, and are such that at a given r, $m = 0$, 2 for a pure mode II stress state with positive, negative shear, respectively, and $m = 1$, 3 for a pure mode I stress state with tension, compression, respectively. Likewise, different values of n and l can be appropriately interpreted. In the present work, values of the mode-mix functions in the full range of one period will be used.

When both the materials are linear elastic, the functions $m(r)$, $n(r)$, and $l(r)$ can be evaluated from the available analytical solution to the elastic interfacial crack problem [eqn (7)]. In that case, denoting $m(r = L)$ by m_{el}, the elastic phase angle ψ satisfies $m_{el} = 1-(2/\pi)\psi$. In the rest of this paper, the subscript "*el*" will be associated with the elastic fields. In the context of the small scale yielding problem, m_{el} (or ψ) measures the mode mix of the elastic fields that are imposed in the far field as boundary conditions. The far-field elastic mode mix m_{el} can take on any value between 0 and 4 (considering one full period), depending on the proportions of tension and shear of the applied loading.

The quantities $m_{pl} = \lim_{r\to 0} m(r)$, $n_{pl} = \lim_{r\to 0} n(r)$, and $l_{pl} = \lim_{r\to 0} l(r)$, on the other hand, define three measures of mode mix at the crack tip ($r \to 0$). The ductile material particles close to the crack tip can be expected to yield plastically due to the singular nature of the stress fields, and the subscript "*pl*" will be associated with the elastoplastic fields in the immediate vicinity of the crack tip. As discussed earlier, an asymptotic analysis of the problem suggests that only four near-tip solutions of the form (13) and (14) are possible. Hence, each of the quantities m_{pl}, n_{pl} and l_{pl} can only take on one of four values. The near-tip "tensile" (or "compressive") asymptotic solution has an associated $m_{pl} \approx 1$ (or 3), and the near-tip "positive-shear" (or "negative-shear") asymptotic solution has an associated $m_{pl} \approx 0$ (or 2). In general, no intermediate values are possible.

The discussion in the above paragraphs suggest that, in the presence of plasticity, the near-tip mode mix, as quantified by m_{pl}, n_{pl}, and l_{pl} is, to a large extent, independent of the applied elastic mode-mix m_{el}. It appears that, the effect of the remote loading is felt at the crack tip primarily through the plastic intensity factor.

2.3. *Plastic stress intensity factor*

An asymptotic analysis only provides partial (although crucial) information about the near-tip fields. The amplitude of the near-tip fields, K_{pl}, cannot be determined from the results of the asymptotic analysis alone. The solution of the small scale yielding problem is necessary to determine K_{pl}, and in this section, the procedure for determining K_{pl} from the small scale yielding results is briefly outlined. To this end it is useful to introduce, following Sharma et al. (1993), the functions:

$$B_{ij}(r,\theta) = \sigma_{ij}(r,\theta)/(2\pi r)^s \tilde{\sigma}^0_{ij}(r,\theta) \tag{18}$$

where $\sigma_{ij}(r,\theta)$ ($ij = xx$, yy, xy, and zz) are the stress components as obtained from the small scale yielding results for a given ψ, s is the strength of singularity of either the "tensile" (or "compressive"), or the "positive-shear" (or "negative-shear") near-tip solution, and is known from the results of the asymptotic analysis, and $\tilde{\sigma}^0_{ij}(\theta)$ are the appropriate asymptotic angular variations, also known from the results of the asymptotic analysis.

For a given ψ, if the small scale yielding stress field $\sigma_{ij}(r,\theta)$ is of the variable-separable form (13), then, $\lim_{r\to 0} B_{ij}(r,\theta)$ is independent of the specific ij-combination, and θ, and is equal to K_{pl}.

Depending on the near-tip stress state, K_{pl} may be thought of as either the "tensile", or the "shear" plastic stress intensity factor (see BPC). Thus, for a given ψ we expect:

$$\lim_{r\to 0} B_{ij}(r,\theta) = K_{pl} \quad \forall i,j,\theta \tag{19}$$

to yield either the "tensile", or the "shear" plastic stress intensity factor. Thus, the determination of K_{pl} requires both the small scale yielding and the asymptotic results. Note that, relations similar to (18) and (19) can also be defined in terms of the components of the stress deviator tensor, and those of the velocity vector.

Since the results of the asymptotic analysis suggest that the near-tip fields are affected by the remote loading fields, to a large extent, only through the plastic stress intensity factor; it is natural to expect K_{pl} to be a function of ψ.

2.4. *A summary of the objectives of the small scale yielding analysis*

The solutions [relations (13) and (14)] to the asymptotic problem represent only a special class of functions, namely those variable-separable in r and θ. The possibility of non variable-separable near-tip solutions was not explored in the asymptotic analysis. If solutions of the latter kind exist near the crack tip, the finite element small scale yielding results can be expected to capture them. If on the other hand, the near-tip solutions as predicted by the results of a full-field finite element analysis are of the variable-separable type only, these results can be expected to (i) verify whether such near-tip variable-separable solutions correspond to one of the four stress states predicted by the asymptotic analysis; (ii) determine the plastic stress intensity factor as a function of the applied mode mix; (iii) determine the regions of validity of the near-tip states as a function of the applied mode mix; and (iv) lead to connections between applied loading fields and the near-tip states, and thus aid in the physical interpretation of the results in predicting the overall behavior of a steadily growing crack subjected to mixed-mode loading conditions. In particular, the remote loading fields that lead to compressive near-tip stress-states may yield insight towards the possibility of crack-tip shielding.

3. Small scale yielding results

The results of the small scale yielding problem are presented in several sub-sections. First, the radial variations of the mode mix functions (15)–(17) are studied, with particular emphasis on their near-tip behavior relative to the remote loading fields. Next, the plastic zones at the crack tip are examined. Subsequently, the plastic stress intensity factor is first estimated based on the limiting process (19), and is then used to supplement the asymptotic solutions in evaluating the radial and angular variation of the asymptotic stress and velocity fields, respectively, for given values of r and θ. The latter facilitates comparisons between the numerical results of the present work and the analytical asymptotic solutions obtained earlier.

3.1. *Radial variation of the mode mix functions*

Far from the crack tip, the mode mix is equal to the value that is imposed as a boundary condition, and hence can vary. For example, m_{el} can vary continuously between 0 and 4. On the other hand, the results of the asymptotic analysis predict that the near-tip mode mix does not vary continuously, and takes on only one of four discrete values. The above observations suggest that, the small scale yielding solutions for a wide range of values of the remote mode mix are likely to share a common near-tip behavior—namely, one of the four values of the near-tip mode mix predicted by the asymptotic analysis. The plastic stress intensity factor, however, can vary with the remote mode mix. The issue that becomes important next is determining the connections among the remote and the near-tip fields. Based on such connections, qualitative predictions can be made about the behavior of the growing crack as the remote mode mix varies. In particular, for crack growth along a brittle/ductile interface, the remote loading conditions that lead to a near-tip tensile or positive-shear state should facilitate further crack growth, while the remote conditions that lead to a compressive or negative-shear near-tip state should lead to crack closure.

Before getting into specific details of the results, some general observations are made on the manner in which the plots are presented. Separate figures are presented for each of the functions $m(r)$, $n(r)$, and $l(r)$, respectively: each function plotted vs $\log(r)$, where we recall that r is normalized such that $r_p = 1$. In each figure, plots are shown for a series of values of ψ, which is noted at the right side of each plot. The known asymptotic near-tip predictions are also shown in each figure using the symbols $a_{pl}(T)$, $a_{pl}(C)$, $a_{pl}(S^+)$, and $a_{pl}(s^-)$ ($a = m$, n, or l), for the near-tip tensile, compressive, positive-shear, and negative-shear solutions, respectively. Finally, in some of the plots the behavior of the mode mix functions in the absence of plasticity is also shown. The latter serves to emphasize the fundamental differences between the near-tip behavior with, and without plasticity.

Figure 2(a)–(b) show radial variations of the function m. For ψ in the range $[-22.5^\circ, 67.5^\circ]$ (see Fig. 2(a)), all the curves strongly converge towards the near-tip "tensile" solution ($m_{pl}(T) = 0.923$). The above range of values of ψ corresponds to primarily remote tension ($\psi = 0^\circ$), with increasing positive shear for increasing values of ψ, and increasing negative shear for decreasing values of ψ. In the above range, the small scale yielding results are in strong support of one aspect of the asymptotic predictions, namely that, the near-tip mode mix is independent of the applied mode mix. The results also predict that a far-field loading that is predominantly tensile or positive-shear is likely to lead to a near-tip "tensile" state.

The dashed curves in Fig. 2(a) are the analytical results in the absence of plasticity. It can be shown that these curves are straight lines with a slope of $-\varepsilon$ (which is known to be small here). Clearly, the behavior of the mode-mix functions is markedly different in the absence of plasticity. In particular, close to the crack tip the functions in the absence of plasticity do not converge towards a single value. In the absence of plasticity, the near-tip mode mix strongly depends on the remotely applied value.

Figure 2(b) shows results for increasing applied positive shear, and, for values of $\psi > 90^\circ$, positive shear mixed with compression. The curve for $\psi = 67.5^\circ$ is repeated for the sake of continuity with Fig. 2(a). A sharp transition is observed in the near-tip behavior of the mode mix as the applied mode mix angle ψ changes from 67.5–90°. From a state of tension, the near-tip state switches to a state of compression. A comparison between Fig. 2(a) and (b) indicates that depending

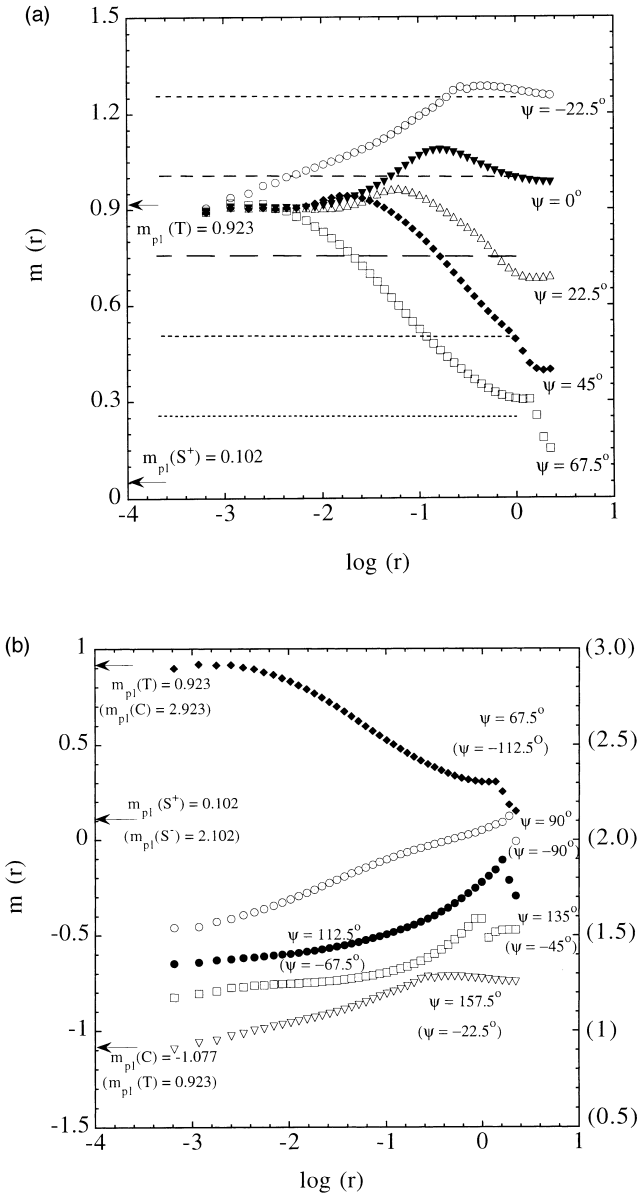

Fig. 2. Radial variations of the mode mix function $m(r)$. (a) For remote tension mixed with positive shear ($\psi > 0^\circ$), and negative shear ($\psi < 0^\circ$). (The results in the absence of plasticity are shown with dashed lines.) (b) For remote positive shear mixed with tension ($\psi < 90^\circ$) and compression (for $\psi > 90^\circ$). (Note that the near tip behavior switches from "tensile" to a transitory "shear" to eventually a "compressive" state.) Each curve corresponds to two different values of ψ, one is enclosed in parenthesis, while the other is not.

on the sign of the change, a change of 22.5° in the value of ψ about $\psi = 67.5^\circ$ can lead to quite disproportionate changes in m_{pl}. Thus, there is hardly any change in m_{pl} as ψ decreases from 67.5–45°. However, the corresponding change is substantial as ψ increases from 67.5–90°. The change

is even more significant physically, because a tensile near-tip state is expected to lead to opening of the crack, while a compressive near-tip state is expected to lead to crack closure. A compressive near-tip state is observed even for $\psi > 90^\circ$. Sufficiently close to the crack tip, these curves will likely approach $m_{pl}(C)(= -1.077)$, which is the mode-mix for the asymptotic compressive solution. This certainly appears to be the case for $\psi = -157.5^\circ$.

Figure 2(b) also shows the corresponding results for far-field loading fields with increasing negative shear, and also for negative shear mixed with compression for $\psi < -90^\circ$. The values of ψ are noted in parenthesis. Note that, the curves for $\psi = -22.5$, -45, -67.5, and -90° can be obtained by applying a shift of $+2$ to the curves for $\psi = 157.5$, 135, 112.5, and 90°, respectively. This is reflected on the right side of the figure where the new values of m: [0.5, 3] are noted. The results suggest that even as the negative shear component of the applied loading increases significantly, the near-tip tensile state is preferred. This is true even for applied pure negative shear ($\psi = -90^\circ$). As ψ decreases from -90 to -112.5°, the near-tip state suddenly switches from tension to compression. Thus, disproportionate changes occur in the value of m_{pl}, as ψ changes by $\pm 22.5^\circ$ about $\psi = -90^\circ$.

Note that, in Fig. 2(a)–(b), results are shown for values of ψ spanning three-quarters of the complete period of $-202.5^\circ \leqslant \psi \leqslant 157.5^\circ$. The quarter-period $-202.5^\circ \leqslant \psi \leqslant -112.5^\circ$ has been omitted in the above presentation because the behavior in the above range is similar to that in the range $-22.5^\circ \leqslant \psi \leqslant 67.5^\circ$, only shifted by $+2$. Thus, in the range $-202.5^\circ \leqslant \psi \leqslant -112.5^\circ$, the near-tip behavior will be compressive—and will lead to crack closure.

The results presented so far provide connections among a wide range of applied loading fields and the associated near-tip states. Next, an attempt is made to interpret these results physically in order to gain further insight into the behavior of a steadily and quasi-statically growing interfacial crack under varying remote mode mix. In the range $-22.5^\circ \leqslant \psi \leqslant 67.5^\circ$, the small scale yielding solutions appear to be strongly attracted (in the sense of a strong convergence) to the near-tip tensile state. The attraction appears to be strongest for $\psi = 22.5^\circ$. It decreases as ψ moves away from 22.5°. More interestingly however, there is a sudden switch in the near-tip state from tension to compression as ψ increases from 67.5–90°. Thus, for values of ψ sufficiently higher than 67.5° the crack tip appears to be shielded from the applied loading fields, because the associated near-tip states, as predicted by the small scale yielding results, are primarily compressive except possibly for a very narrow range between 67.5° and 90° where a positive-shear near-tip state is possible. For negative applied shear, the near-tip behavior of the small scale yielding solutions beyond $\psi = -22.5^\circ$ is somewhat elusive. The finite element results suggest a near-tip tensile state, whereas on physical grounds (considering that the crack is along the interface between a ductile material and a rigid substrate) a negative applied shear can be expected to lead to crack closure. It is possible that the solutions in this range are attracted to a near-tip tensile state at length scales that are so small that any assessment based on such a near-tip behavior may not be physically relevant. Note, however, that the small scale yielding results strongly suggest that out of the four possible near-tip states that were predicted by the asymptotic analysis, either the tensile state or the compressive state is preferred over a significant range of the applied loading fields.

A tensile near-tip state is conducive to further propagation of the crack, whereas a compressive near-tip state is detrimental to it. On the basis of this observation, a far field loading with $\psi = 22.5^\circ$ will be most conducive to crack propagation, and hence will correspond, in some sense, to minimum interfacial toughness. As ψ moves away from 22.5°, it is expected that more energy needs to be

expended to re-orient the fields from their applied mixed-mode states to the near-tip tensile state with an associated $m_{pl}(T)$ that is very different from the applied m_{el}. This can be expected to translate to an increase in the interfacial toughness as ψ moves away from 22.5°. When ψ is sufficiently far from 22.5°, the near-tip state switches from tension to compression, resulting in infinite interfacial toughness (crack closure instead of crack growth). The above qualitative dependence of interfacial toughness on remote mode mix, suggested by the small scale yielding results, is consistent with experimental observations (Cao and Evans, 1989; Liechti and Chai, 1992), and prior theoretical predictions (Liechti and Chai, 1992; TH, Bose and Ponte Castañeda, 1995). It may be noted that, the toughening behavior suggested by the small scale yielding results is related to the fact that the near-tip stress state continues to be tensile or compressive even when the remote stress state is mixed in nature. Recall that the latter is a consequence of plasticity, since in the absence of plasticity the near-tip state is not necessarily tensile or compressive, but varies continuously with a varying remotely applied stress state. This led BPC to refer to this toughening mechanism as a ductile mechanism.

The physical relevance of asymptotic near-tip fields is commonly evaluated (Deng and Rosakis, 1992; Sharma and Aravas, 1993; Omprakash and Narasimhan, 1996) by expressing their regions of validity as a fraction of the crack tip plastic zone size. Under the assumption that the fracture process zone is well embedded within the crack-tip plastic zone, the asymptotic fields are physically relevant if their regions of validity are "significant" fractions of the plastic zone size. From the results presented in this section, an estimate for the region of validity of any one of the four asymptotic states can be obtained by measuring the distance of the point farthest from the crack tip, at which a mode mix function reaches the value of m_{pl} corresponding to that state. The region of validity (for a given near tip state) estimated in the above manner will be a strong function of ψ. In the rest of this section, all estimates for regions of validity will be expressed as fractions of r_p. In the next section the plastic zones at the crack tip will be studied in detail, and the regions of validity will be expressed as fractions of actual sizes of the crack tip plastic zone.

All estimates for the region of validity reported here are expressed on a logarithmic scale. The region of validity of the tensile near-tip state is a maximum for $\psi = 22.5°$, and is equal to -1.5. This is equivalent to about 3% of r_p. It decreases as ψ shifts away from 22.5°, and is equal to -2 (corresponds to 1% of r_p) for both 0 and 45°. There is a sharp decrease in the region of validity of the tensile near-tip state as ψ becomes negative. For $\psi = -22.5°$ it is -3, and decreases further with decreasing ψ. On the other hand, for $\psi > 45°$ the region of validity of the near-tip tensile state also decreases, but less rapidly than it does for negative shear. For $\psi = 67.5°$, the region of validity is -2.5, and for $\psi \geqslant 90°$, the near-tip state switches from tension to compression.

Figure 3 shows the radial variations of the mode mix function $n(r)$ in the range $-22.5° \leqslant \psi \leqslant 67.5°$. Recall that values of ψ in the above range lead to the tensile near-tip state, and hence are important physically. For $0° \leqslant \psi \leqslant 67.5°$, the curves for $n(r)$ converge dramatically towards $n_{pl}(T) = 0.227$. The curve for $\psi = -22.5°$ is flat since the far-field and near-tip values of $n(r)$ are close. The functions in the absence of plasticity are also shown with dashed lines. The difference in the behavior of the mode mix functions with and without plasticity is particularly noticeable in the range $22.5° \leqslant \psi \leqslant 67.5°$. The results with plasticity strongly converge towards the tensile near-tip state, while those in the absence of plasticity do not. The estimates for the region of validity of the near-tip tensile state are also consistent with prior estimates obtained from the results for the function $m(r)$.

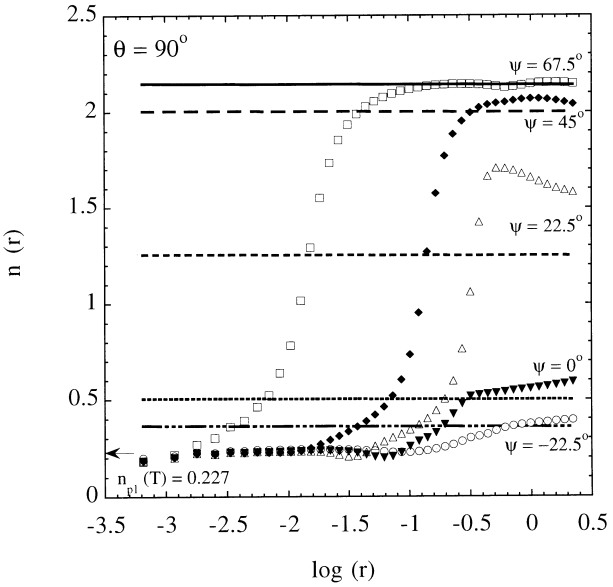

Fig. 3. Radial variations for the functions $n(r)$ for the range of remote loadings (ψ) that leads to a near-tip tensile state. The results in the absence of plasticity are also shown with dashed lines.

Figure 4 shows the corresponding results for the function $l(r)$, both with and without plasticity, in the range $-22.5^\circ \leqslant \psi \leqslant 67.5^\circ$. In the presence of plasticity, all the curves converge towards $l_{pl}(T) = 2.692$.

In conclusion, the near-tip limits of the small scale yielding results are fairly consistent with the predictions of the asymptotic analysis. In particular, the near-tip mode-mix appears to be independent of the far-field mode-mix over significantly wide ranges of the applied loading fields. The tensile/compressive near-tip states appear to be preferred over the positive/negative shear near-tip states. Finally, the connections between the near-tip and the remote states obtained from the results in this section are suggestive of a ductile mechanism to explain the dependence of interfacial toughness on the mode mix of the applied loading fields.

3.2. *Near-tip plastic zones and effective stress histories of material particles*

In this section, the active plastic zones for $-22.5^\circ \leqslant \psi \leqslant 45^\circ$ are presented. Recall that, in the above range of the remote loading fields, the near-tip stress state is tensile. The analytical results for the elastic unloading and plastic reloading angles (see PCM) for a typical material particle close to the crack tip are known from the asymptotic analysis, and these can be compared with the corresponding small scale yielding results. The regions of validities of the asymptotic results, which were expressed earlier as fractions of r_p, are assessed against the crack tip plastic zone sizes.

Figure 5(a)–(d) show the plastic zones for $-22.5^\circ \leqslant \psi \leqslant 45^\circ$. Note that in Fig. 5(a), which shows results for $\psi = -22.5^\circ$, and in all subsequent plots for the plastic zones, the crack lies along the negative x_1 axis, with the crack tip at $(0, 0)$. The dotted regions represent material particles that are actively yielding, while the plain regions represent material particles that are currently

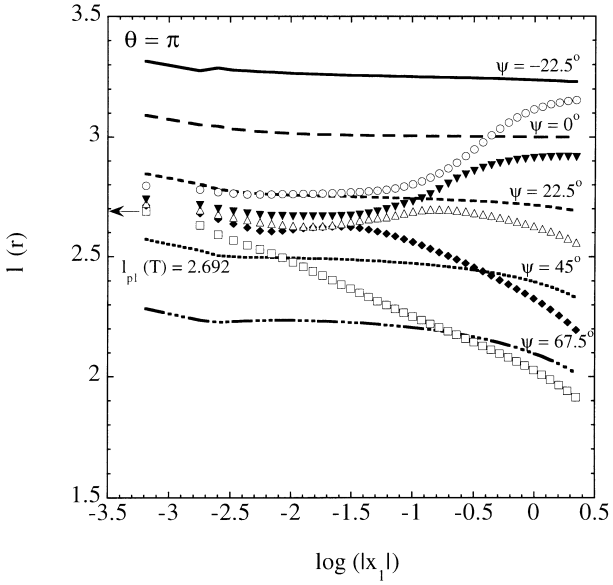

Fig. 4. Radial variations of the functions $l(r)$ for far field loading fields (ψ) that lead to a near-tip tensile state. The results in the absence of plasticity are also shown with dashed lines.

deforming elastically. The regions can be distinguished more precisely based on the deformation history of material particles as the crack tip moves past these particles. In front of the crack and far away from it, corresponding to large positive values of x_1, a material particle begins loading elastically (based on the assumption that the material ahead of the crack is in an unstressed state). As the crack moves forward, the same material particle comes closer to the crack tip, and, provided that it is sufficiently close to the crack plane in the x_2 direction (for example, less than $x_2 = 0.5$ in Fig. 5(a)), it yields plastically due to the singular nature of the stresses close to the tip. This initial yielding results in a primary plastic zone (the vertical dotted "leaf" in Fig. 5(a)). As the crack tip travels further, the same particle begins unloading elastically. This leads to the white region to the immediate left of the primary plastic zone. The material particle may reload plastically as it moves into the wake of the crack, if its effective stress reaches the current yield stress. This results in a secondary plastic zone (the thin dotted region attached to the upper crack face in Fig. 5(a)). While most of the plastic zones at the tip of a growing crack follow the above pattern, there are some exceptions. An exception occurs for the case presented in Fig. 5(a) (not visible in the scale of the figure), in the form of an "additional" tiny region of actively yielding material extending roughly from $x_1 = 0.1$ to $x_1 = 0.25$. The origin of the additional plastic zone will become apparent from a study of the effective stress history of a material particle as the crack tip moves past the particle. This is discussed later in this sub-section. Figure 5(b)–(d) show the evolution of the plastic zones at ψ increases. The result suggest that the effects of increasing positive shear are (i) to shift the primary plastic zone to the right (in the direction of the positive shear force), and (ii) to result in an overall increase in the size of the primary plastic zone, the increase being particularly noticeable in the transition from 22.5–45°. The latter observation is consistent with the results of Leichti and Chai (1992), where the authors noticed that the plastically deformed region under bond-normal

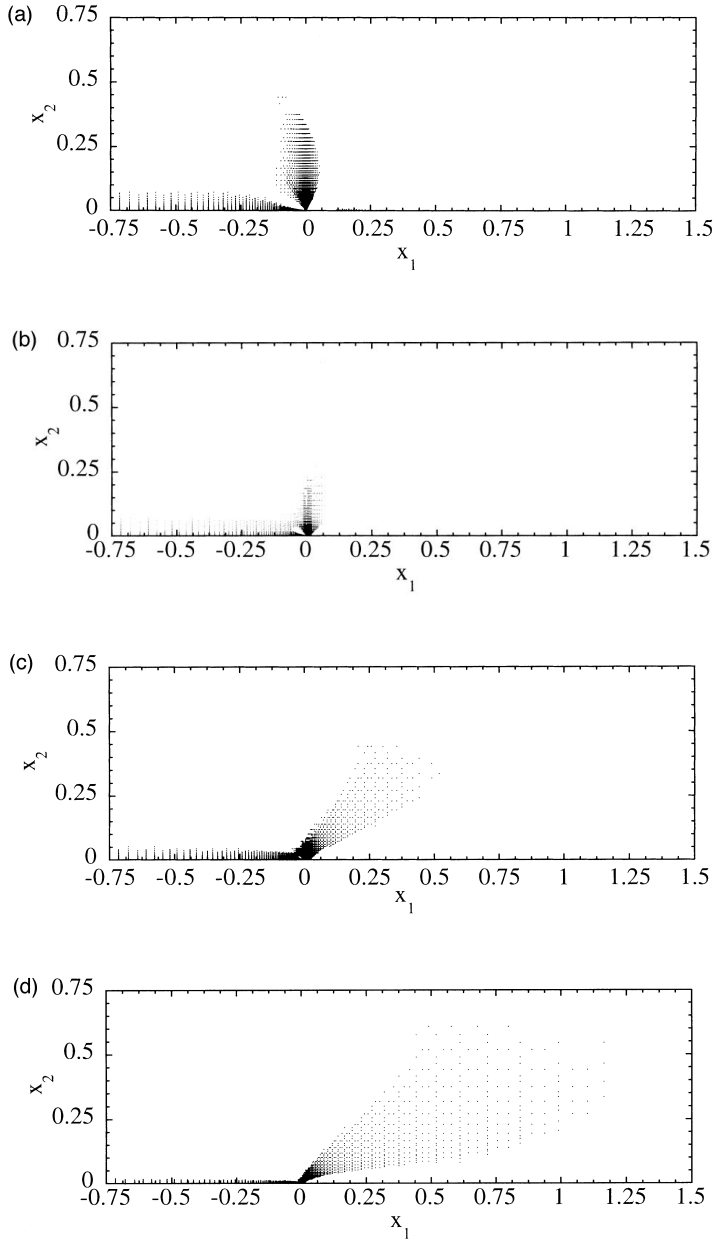

Fig. 5. (a)–(d) : Active plastic zones for $\psi = -22.5$, 0, 22.5, and 45°, respectively.

loading is extremely small in comparison to the plastic zones that developed under bond-tangential loadings. The height of the secondary plastic zones on the other hand appears to be decreasing with increasing positive shear. Note that in the above plots, the full extent of the secondary plastic zone (usually till $x_1 \approx -8$) is not shown. The size of the plastic zone is often considered to provide

a measure of the amount of plastic dissipation at the crack tip (see Leichti and Hanson, 1988). If the plastic dissipation is directly proportional to the size of the plastic zone, then it could potentially account for the increase in interfacial toughness with shear. Liechti and Chai (1992) estimated the rate of plastic dissipation during crack initiation. They also considered the effects of viscoelastic dissipation and interfacial asperity shielding, and concluded that even the combined effects of all three factors did not account for the sharp increase of toughness with increasing shear.

Figure 6(a)–(d) show enlargements of the plastic zones in the immediate vicinity of the crack tip for $-22.5^\circ \leqslant \psi \leqslant 45^\circ$. Two lines, showing the asymptotic predictions for unloading (continuous line) and reloading (broken line), respectively, are also included in each plot. Although the asymptotic unloading and reloading angles do not agree precisely with the finite element results, the angular extent of the intermediate elastic region appears to be in reasonably good agreement.

Figure 7 shows the effective stress history of a material particle as it approaches the crack tip and then moves away from it. The height of the particle above the interface is given by $x_2 \approx 2.5 \times 10^{-3}$. The remote loading field corresponds to $\psi = -22.5^\circ$. The curve has three peaks, two of which can be seen in this plot. The first peak is close to $x_1 = 0.1$, while the second peak occurs at a very small negative value of x_1. The first peak is such that σ_e exceeds the initial yield stress $\sigma_0 = \sqrt{3}\tau_0 = 0.01732$, before the peak is reached. The particle unloads at this peak where $\dot{\sigma}_e = V(\sigma_e)_{,1} = 0$. This leads to the small plastic zone between $0.1 \leqslant x_1 \leqslant 0.25$, which was referred to as the "additional" plastic zone in a previous paragraph. This "additional" zone is an exception, and is followed by the more common pattern of deformation history leading to primary and secondary plastic zones, respectively. In fact, the effective stress boundary history of a material particle has three peaks for all values of ψ for which results are presented in this section (the plots for other values of ψ are not shown here). However, the value attained by σ_e at its first peak is well below σ_0 in all the other cases, and hence there is no "additional" plastic zone.

The corresponding results for $\psi = 67.5^\circ$ (not shown here) are similar. However, due to a decrease in the region of validity of the asymptotic tensile solution, the asymptotic unloading and reloading angles do not compare well with the finite element results. In the latter case, a better comparison may result from further resolution of the near-tip region.

The regions of validity of the asymptotic fields can be expressed as fractions of the actual sizes of the crack-tip plastic zones. Thus, for $\psi = 22.5^\circ$ the region of validity is approximately 3% of r_p $(=1)$. In terms of the maximum size of the actual plastic zone (see Fig. 5(c)), which is approximately 0.6 for this case, the region of validity is about 5%. The relative size of the region of validity of the asymptotic fields for neighboring values of ψ is similar, but it decreases for more extreme values of ψ. In this context, it is relevant to mention that McClintock and Argon (1966—see Figure 16.13 in this reference) show an example of a cracked structure, with the crack-tip region viewed at progressively coarser length scales. The grains, inclusions, and voids are at a distance (from the crack tip) of 10^{-3} cm or even lower, as compared to the elastic singularity at a distance of 1 cm. Assuming that the fracture mechanism is primarily growth and coalescence of voids occurring at length scales comparable to those suggested by McClintock and Argon, the regions of validity of our near-tip asymptotic fields for the steadily growing crack can thus be seen to be physically relevant.

However, it should be noted that, without a conservation integral to determine the stress intensity factor, the near-tip solutions cannot be used in the same manner as the HRR (Hutchinson, 1968; Rice and Rosengren, 1968) singularity fields for a stationary crack. However, the near-tip

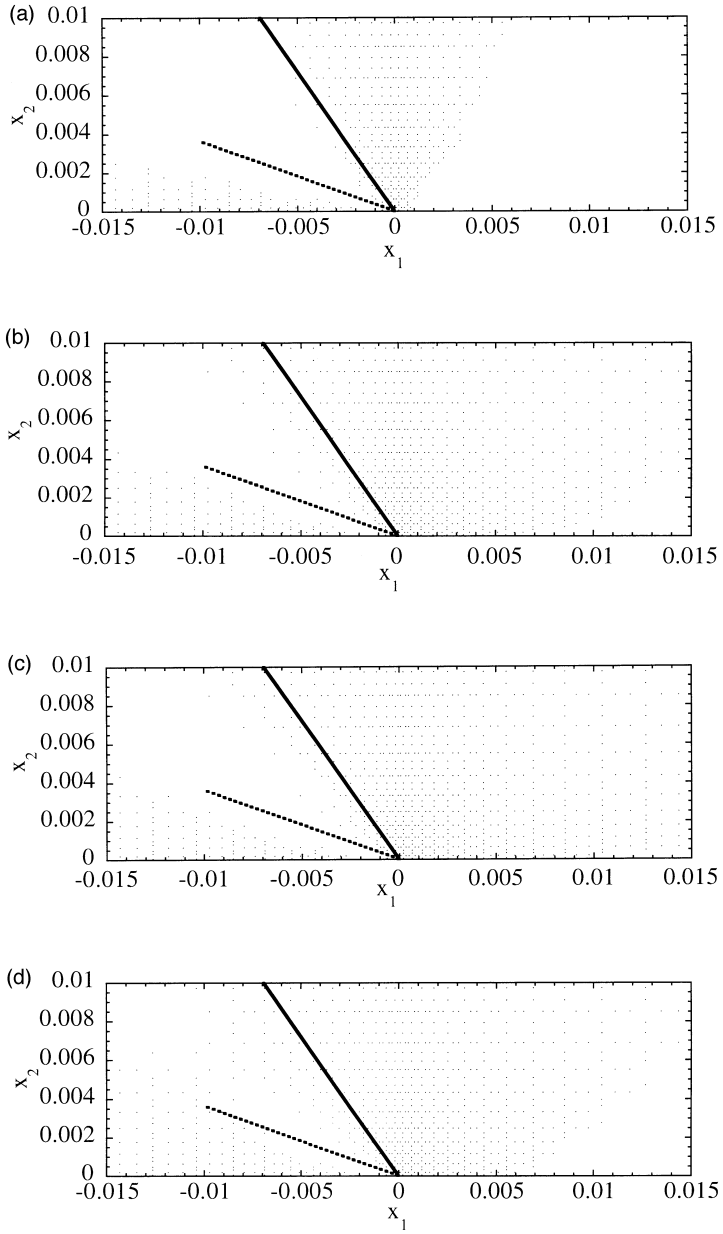

Fig. 6. (a)–(d): Near-tip regions magnified to show comparisons between the finite element (for $\psi = -22.5$, 0, 22.5, and 45°, respectively) results and the prediction from the asymptotic analysis for the "tensile" near-tip solution. The asymptotic elastic unloading and plastic reloading angles are shown with continuous and broken lines, respectively.

asymptotic solutions for the steadily propagating crack do predict, rather accurately, certain important information about the problem, such as the near-tip mode mix. In addition, as shown in a later section of this paper, they suggest the potential usefulness of a standard crack growth

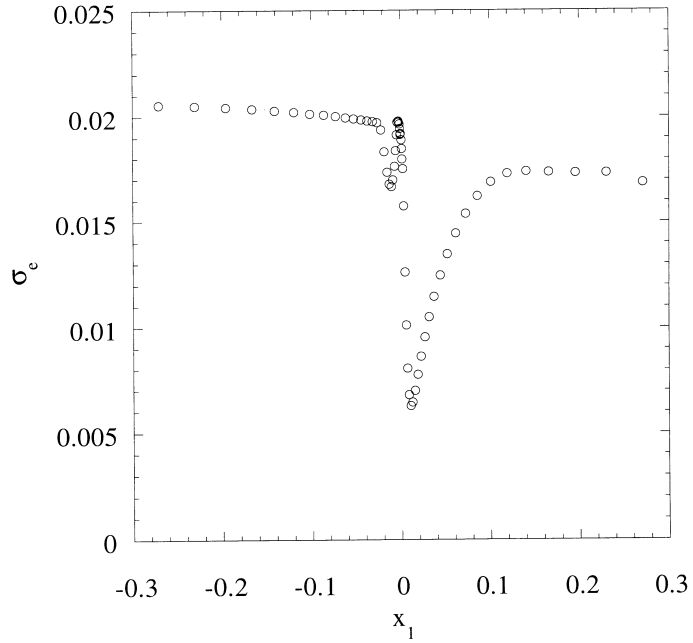

Fig. 7. Effective stress history of a material particle as the crack tip moves past it.

criterion (the use of which obviates the need to stipulate critical conditions on the near-tip deformation fields) in the context of predicting the dependence of interfacial toughness on mode mix, at least for relatively strong interfaces. Finally, given that the numerical simulation of crack growth problems is notoriously difficult, it is helpful to have asymptotic fields to check the numerical simulations against. At the very least, the near-tip asymptotic solutions of this work could be used in such a manner.

3.3. *Plastic stress intensity factor*

The functions $B_{ij}(r,\theta)$ defined by relation (18) are evaluated for different values of ψ. The known analytical results for the asymptotic tensile solution provide some of the ingredients necessary in evaluating $B_{ij}(r,\theta)$. Figure 8 shows the radial variations of B_{yy} at several values of θ, for $\psi = 22.5^\circ$. Far from the crack tip the elastic singular fields dominate, and hence B_{yy} is a function of θ. As the crack tip is approached, the functions at different values of θ appear to converge within a narrow band and flatten out. This behavior corresponds to a tendency of the functions to approach a limiting value that is independent of θ as $r \to 0$. This limiting value is the plastic stress intensity factor, K_{pl}, for $\psi = 22.5^\circ$. It can likewise be evaluated at other values of ψ (the details are not presented here). Theoretically, at a given value of ψ, the limit for $B_{ij}(r,\theta)$ should be independent of the *-ij-* component and the angle θ. Numerically, however, the predictions for K_{pl} depend on these factors. The variations in K_{pl} with these factors are fairly small for values of ψ close to 22.5°, where the asymptotic tensile field has fairly large ranges of validity. The variations increase as the region of dominance of the asymptotic tensile field decreases. For consistency, in all subsequent

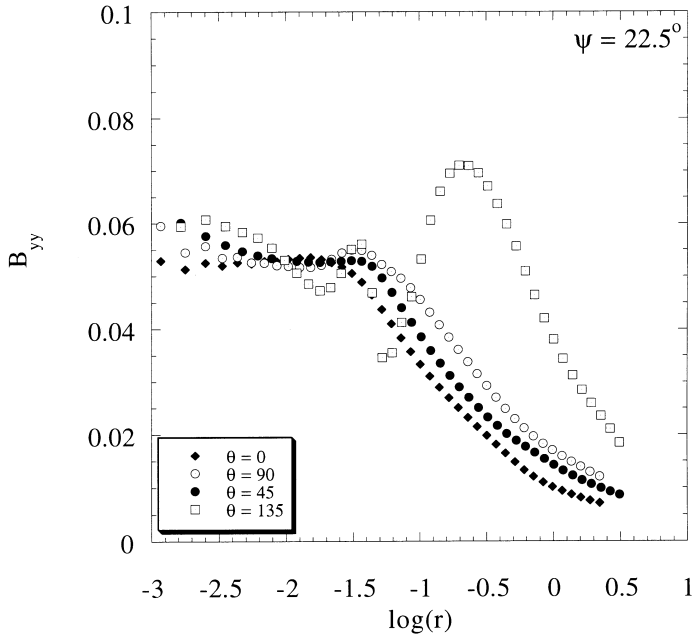

Fig. 8. Radial variations of the function B_{yy} at several values of θ and for $\psi = 22.5^\circ$.

calculations utilizing the plastic stress intensity factor, the value of B_{xx} at $\theta = 90^\circ$ and at the fourth data point (from the crack tip) is used as K_{pl}.

3.4. *Radial variations of the stresses*

If the stress fields are variable-separable and power singular in r, then, on a log–log plot of σ_{ij} vs r for given values of θ and ψ, a stress field of the form (13) would appear as a straight line with slope s. However, in order to evaluate (13), the asymptotic results need to be supplemented by $K_{pl}(\psi)$. On the other hand, the elastic fields are not variable-separable for non-zero values of ε, and hence a log–log plot of σ_{ij} vs r (for given values of θ and ψ) will be a curve and not a straight line. However, as the results to be presented next illustrate, for sufficiently small values of ε the curves appear as straight lines. In order to satisfy the imposed boundary conditions of the small scale yielding problem in the far-field ($r \to \infty$), the finite element results for $\log \sigma_{ij}$ vs $\log r$ remote from the crack tip can be expected to be coincident with the corresponding elastic results. Likewise, close to the crack tip ($r \to 0$) the finite element results can be expected to be identical to the line representing the asymptotic stress state.

In this section the radial variations of the stresses obtained from three different sources are presented. These are the asymptotic elastoplastic, the linear-elastic, and the finite element stress fields, respectively. The radial distance r is normalized such that $r_p = 1$. In each plot, results from all three sources are shown. The finite element results are shown with open circles, the asymptotic results with continuous lines, and the linear elastic results with broken lines. It should be noted that, for a given value of ψ all asymptotic stress components are computed based on a single value

of K_{pl}, namely, that given by the limit (as $r \to 0$) of B_{xx} at $\theta = 90^\circ$. Thus, the results can be expected to provide an overall check on the near-tip variations as predicted by the asymptotic analysis. The above method for presenting the radial variations of the stress fields has the following advantages. Firstly, close to the crack tip, the extent to which the finite element results approach the asymptotic predictions can be assessed. Secondly, the distance from the crack tip over which good agreements are observed between the finite element and the asymptotic results will provide another estimate of the region of validity of the asymptotic fields. Finally, these plots can also provide valuable information on the behavior of the stress fields at "intermediate" (regions that fall between the near-tip and the far-field) distances from the crack tip. The latter can be important in determining the relevance of higher order terms in the near-tip asymptotic expansion of stress fields (O'Dowd and Shih, 1991, 1992; Sharma et al., 1995).

Figure (9) shows radial variations of σ_{yy} and σ_{xx} at $\psi = 0^\circ$. The figure is further sub-divided into four parts (a)–(d); with (a)–(b) showing radial variations of σ_{yy} at $\theta = 0^\circ$, and 90°, respectively; and (c)–(d) showing radial variations of σ_{xx} at $\theta = 45$ and 135°, respectively. In the following discussion, the important features of Fig. 9(a) are highlighted with the understanding that similar observations also hold for all the other figures in this section.

The most important point to note from Fig. 9(a) is the bi-linear nature of the finite element stress field. Close to the crack tip, the finite element results are on top of the line representing the asymptotic near-tip solution; while, remote from the crack tip they are on top of the line representing the elastic solution. Another important observation is that close to the crack tip, the slope of the line corresponding to the finite element results is close to the slope of the line representing the asymptotic solution. The above observations have the following implications. The linear near-tip behavior of the small scale yielding stress fields in the figure suggests variable-separability of the power singular type as $r \to 0$. The fact that the slopes are close implies that the strength of the singularity of the stress fields, as computed from the small scale yielding results, is close to the corresponding asymptotic prediction, s. These observations confirm that the stress fields close to the crack tip are indeed given by the asymptotic results (13). It may be noted that good agreements are observed between the finite element and the asymptotic results up to a distance of -1.5 on the logarithmic scale. This provides yet another estimate of the region of validity of the asymptotic tensile stress state.

The results for $\psi = 22.5^\circ$ (not shown here; see Bose (1995) for further details) are not significantly different from the corresponding results for $\psi = 0^\circ$. The region of validity of the tensile asymptotic solution, as predicted by these results, is between -1.5 and -1 on the logarithmic scale. For $\psi = 45^\circ$, there is a significant decrease in the region of validity of the asymptotic tensile solution to approximately -2 on the logarithmic scale. Thus, the region of validity appears to be a strong function of ψ, and the dependence on ψ is consistent with that obtained from the results for the mode mix functions.

3.5. *Angular variations of stress fields*

In this subsection, the small scale yielding stress-deviator fields are plotted along a contour surrounding the crack tip, and the results are compared against the corresponding asymptotic fields along the same contour. For the finite element mesh used, it is a matter of convenience to choose data points along a half-square contour that surrounds the crack tip in the ductile material

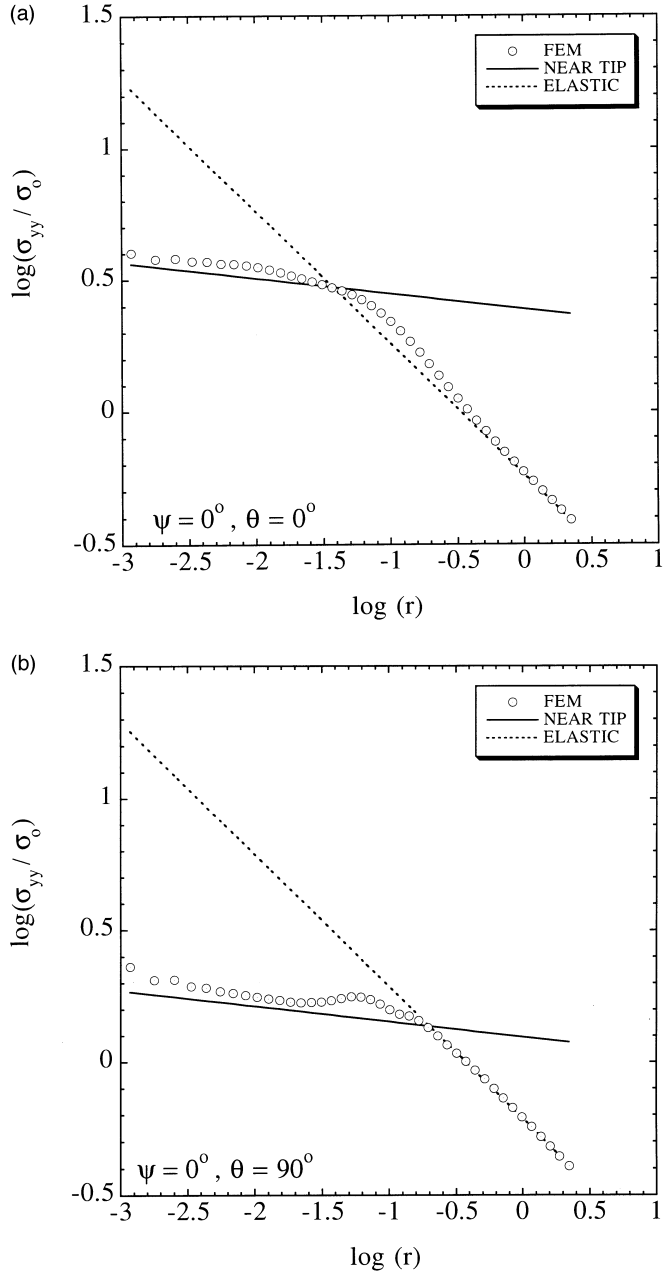

Fig. 9. (a)–(b): Radial variations of stress component σ_{yy} at $\theta = 0$ and 90°, respectively, for a far-field loading with $\psi = 0°$; (c)–(d): corresponding results for σ_{xx} at $\theta = 45$ and 135°, respectively. In all the plots, the open circles represent the finite element results, the continuous lines represent the asymptotic near-tip stress state (tensile), and the broken lines represent the elastic stress fields. The radial distance r is normalized such that $r_p = 1$.

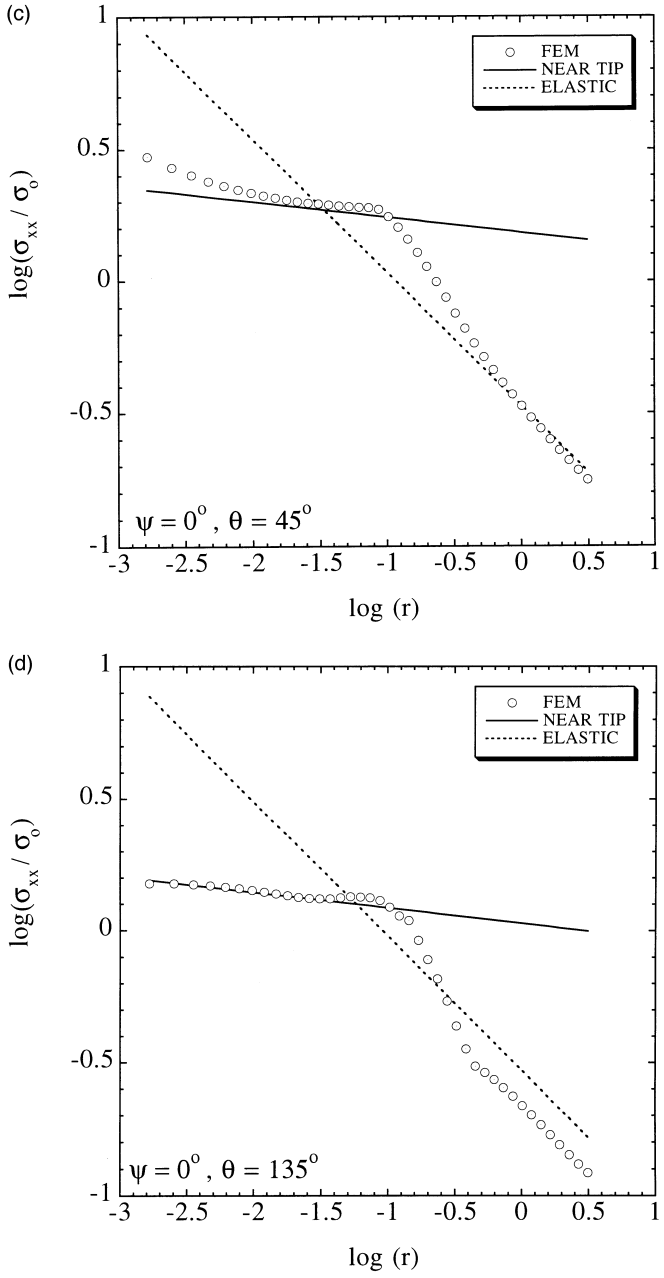

Fig. 9.—*Continued.*

(upper half plane). The average distance of the contour from the crack tip is approximately a fraction of a percent of r_p. Thus, the contour is well within the plastic zone for most values of $0 \leqslant \theta \leqslant \pi$. In terms of the finite element mesh, the contour is the fifth square "emanating" from

the crack tip (see Dean and Hutchinson, 1981, for a similar approach). It may be noted that the angular variations of the fields, as extracted in the above manner, do not correspond to a fixed value of r, and hence cannot be directly compared to the deviators derived from the known angular variations $\tilde{\sigma}^0_{ij}(\theta)$ of the asymptotic stress field of eqn (13). Instead, eqn (13) is used to compute the deviators at the same values of r and θ for which the finite element results are extracted. It is important to note that, in computing the asymptotic results for the angular variations of the stress deviators for a given value of ψ, a single value of K_{pl} has been used for computing all the deviator components. This value is the limit (as $r \to 0$) of B_{xx} at $\theta = 90^\circ$. In the results to follow, the finite element results are shown with open circles, while the asymptotic results are shown with continuous lines.

Figure 10(a)–(c) show the results for the stress deviator components s_{yy}, s_{xx}, and s_{xy} $(=\sigma_{xy})$, respectively. In each plot the finite element results are shown for $\psi = 0$, 22.5, and 45°, respectively, and the tensile asymptotic solution is superposed on the finite element results with a continuous line. The results indicate that the angular variations of the stress deviator fields are invariant to changes in ψ except for a tiny shift (barely noticeable on the scale of the figures) due to different values of K_{pl}. This behavior of the small scale yielding results suggests that the effect of the far-field mode mix is felt at the crack tip only through K_{pl}. This is in agreement with the predictions of the asymptotic analysis. The finite element results are in good agreement with the asymptotic results for all values of θ outside the range $150^\circ \leqslant \theta \leqslant 180^\circ$. Between 150 and 180° the finite element results for s_{yy} and s_{xx} appear to be different from the corresponding asymptotic predictions.

The finite element results for $\psi = 67.5$ and -22.5° (not shown here) are also in good agreement with the tensile asymptotic solution.

3.6. *Near-tip shear solution*

Referring back to Fig. 2(b), note that a sharp transition occurs in the near-tip behavior of the mode mix functions (and hence the stress fields) as ψ changes from 67.5–90°. While the near-tip stress state for $\psi = 67.5^\circ$ is predominantly tensile, that for $\psi = 90^\circ$ is compressive. This suggests the possibility of a near-tip "positive-shear" state for some values of ψ between 67.5 and 90°. A closer inspection of the mode-mix functions in the above range of values of ψ (Fig. 11) reveals that for $\psi = 83.7^\circ$ the near-tip stress state is in good agreement with the asymptotic positive-shear solution. However, even for a "small" change in the value of ψ to either 81 or 85.5°, the near-tip state switches from positive-shear to tension, and compression, respectively. Based on the above behavior of the stress fields, it appears that the asymptotic shear state may be "unstable", and may only act as a transitory intermediate state between the "stable" states of near-tip tension, and near-tip compression, respectively. Results for radial and angular variations of the near-tip shear state were obtained in a manner similar to those for a near-tip tensile state. However, for the sake of brevity detailed discussions are omitted here.

While it is not clear as to why the range of remote loading fields for which the near-tip shear state is realized is so narrow, a plausible explanation might be in an inherent tendency of growing cracks to propagate in a manner such that the near-tip fields are of the tensile kind. For cracks propagating in homogeneous materials it is well-known that they reorient their direction of propagation such that the near-tip state is one of mode I. That something similar should happen for an interfacial crack whose direction of propagation is predetermined by the presence of an

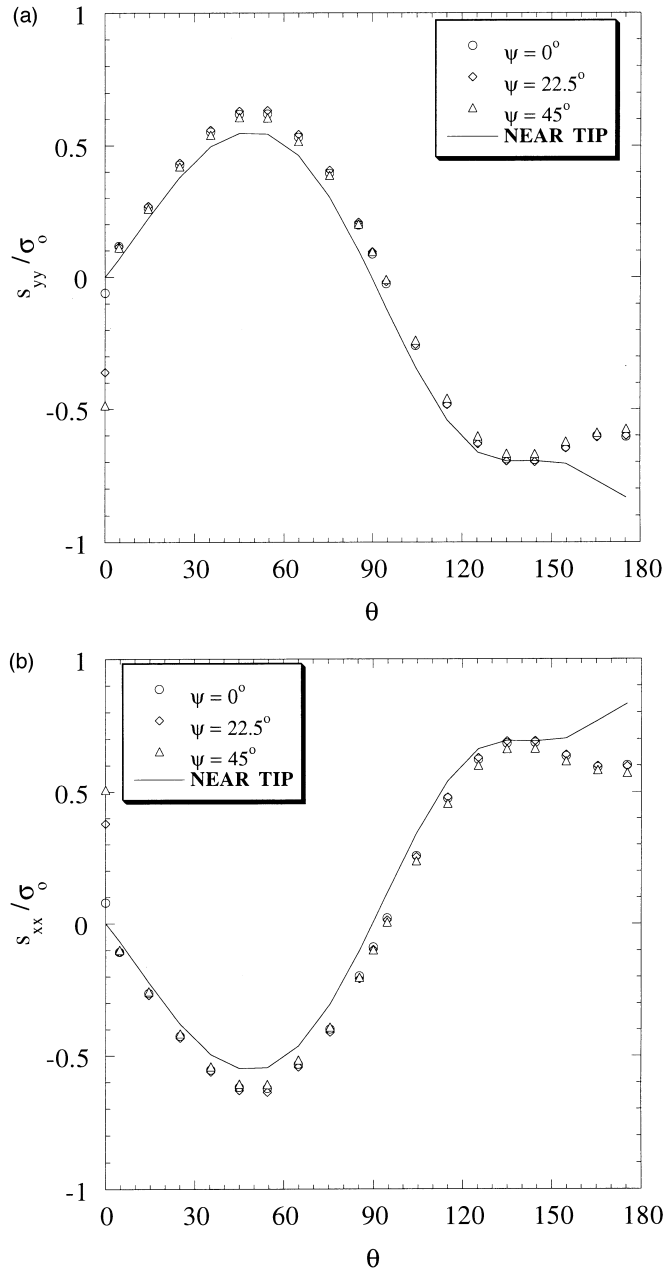

Fig. 10. (a)–(c) : Angular variations of the stress deviator components s_{yy}, s_{xx}, and s_{xy}, respectively. Each plot shows the finite element results for three different mode mix values for which the near tip state is tensile. The continuous line in each plot represents the asymptotic "tensile" solution. The data points are along a square contour that is at an average distance from the crack tip of approximately 0.1% of the plastic zone size.

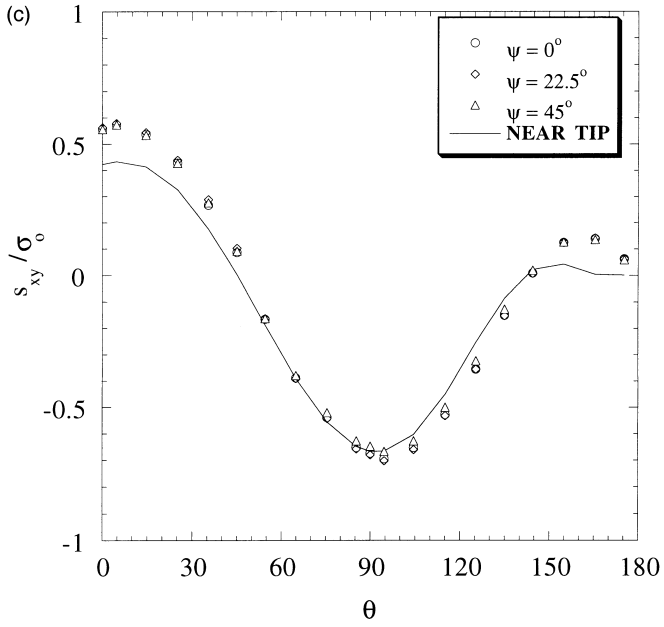

Fig. 10.—*Continued.*

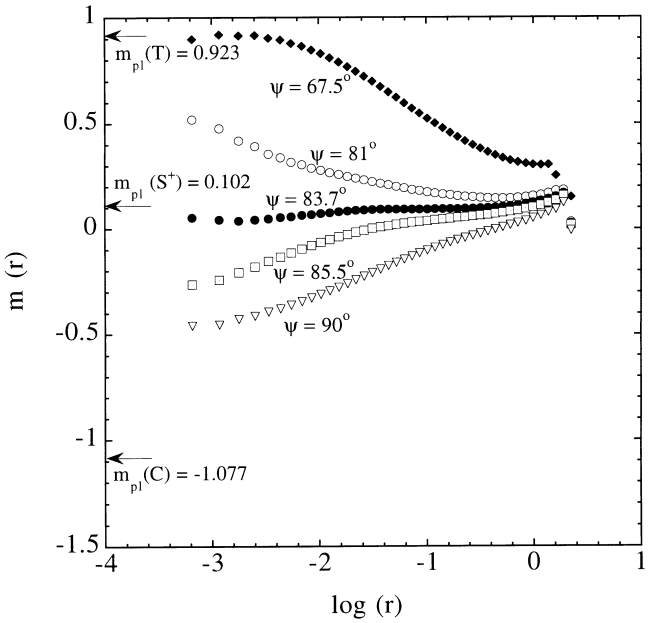

Fig. 11. A closer look at the mode mix function $m(r)$ in the range $67.5^\circ \leqslant \psi \leqslant 90^\circ$. The shear near-tip state results for $\psi = 83.7^\circ$.

interface is by no means obvious. It is possible that this feature is an intrinsic property of the growing crack and only experiments can verify to what extent this is true.

4. Dependence of interfacial toughness on mode-mix: a ductile mechanism

Recent experiments by Cao and Evans (1989) and Liechti and Chai (1991, 1992) indicate that the toughness of an interface may depend strongly on the mode mix of the applied loading fields. This is especially true when at least one of the materials adjacent to the interface is ductile, and the interface itself is strong enough to cause plastic deformation in the ductile phase(s). In this section, we develop further a ductile mechanism, originally proposed by BPC, for explaining this phenomenon in the context of slow crack growth. One of the ingredients of the proposed mechanism is the observation, by PCM (see also BPC), that only four types of asymptotic solutions are possible in the neighborhood of the tip of a crack propagating quasi-statically along the interface between two generally distinct elastoplastic materials. These solutions are "tensile" (or "compressive")- and "positive-shear" (or "negative-shear") like in character, with dominating tensile (or compressive) and shear (positive or negative) stress components, respectively, in the line ahead of the crack. The second ingredient is the observation from the small scale yielding results presented earlier in this paper that the tensile (or compressive)-like near-tip solution is usually preferred to the shear-like solution for fairly large ranges of the prescribed, remotely applied elastic mode mix. Therefore, making the hypothesis that the tensile-like asymptotic solution indeed governs the behavior of the region in the immediate vicinity of the growing crack tip, application of a standard crack growth criterion leads to the requirement that the crack propagate with a fixed near-tip crack opening profile. Imposition of this crack growth criterion results in predictions for the interfacial toughness as a function of the applied mode mix. In the following paragraphs, further details of the mechanism and the predictions for the dependence of interfacial toughness on the applied mode mix, are discussed.

In the development to follow, it is useful to introduce the dimensionless variables

$$\underline{r} = \frac{r}{r_p} \quad \text{(dimensionless radius)}, \tag{20a}$$

$$\underline{\sigma_{ij}} = \frac{\sigma_{ij}}{\tau_0^{(2)}} \quad \text{(dimensionless stress)}, \tag{20b}$$

$$\underline{v_i} = \left(\frac{E^{(2)}}{\tau_0^{(2)}}\right)\frac{v_i}{V} \quad \text{(dimensionless velocity)}, \tag{20c}$$

where $i, j = 1, 2, 3$. The polar angle θ, and the phase angle ψ of the remotely applied elastic singularity fields are dimensionless, by definition.

In terms of these dimensionless variables the remotely applied stress fields (7) may be written as:

$$\underline{\sigma}^{\infty}_{\alpha\beta}(\underline{r}, \theta) = \mathrm{Re}(e^{i(\psi+\varepsilon\ln r)})\underline{r}^{-1/2}\tilde{\sigma}^{\mathrm{I}}_{\alpha\beta}(\theta, \varepsilon) + \mathrm{Im}\,[e^{i(\psi+\varepsilon\ln r)}]\underline{r}^{-1/2}\tilde{\sigma}^{\mathrm{II}}_{\alpha\beta}(\theta, \varepsilon), \tag{21}$$

while the near-tip asymptotic stress state may be written as:

$$\underline{\sigma}^0_{\alpha\beta}(\underline{r},\theta) = \kappa \underline{r}^s \tilde{\sigma}^0_{\alpha\beta}(\theta), \tag{22}$$

where κ is a dimensionless amplitude factor depending on the applied phase angle ψ. From dimensional considerations, it can be shown that, in general, $\kappa = \kappa(\psi; \alpha^{(\alpha)}, \nu^{(\alpha)}, \beta, \lambda)$, where $\lambda = \tau_0^{(1)}/\tau_0^{(2)}$. It is important to emphasize that s and $\tilde{\sigma}^0_{\alpha\beta}(\theta)$ are known from the asymptotic analysis, where κ must be determined from a small scale yielding analysis.

Next, using the definition of the tensile plastic stress intensity factor $K_{pl} = \lim_{r\to 0} \{(2\pi r)^{-s}\sigma_{\theta\theta}(r, \theta = 0)\}$, it can be shown that

$$K_{pl} = \kappa(\psi)(\tau_0^{(2)})^{2s+1}(K_{el})^{-2s} \tag{23}$$

so that κ is a dimensionless plastic stress intensity factor serving to determine K_{pl}.

The small scale yielding results presented earlier determine K_{pl} as a function of ψ for the ductile/brittle material pair considered. This in conjunction with relation (23) determines κ as a function of ψ.

4.1. *Crack growth criterion*

Given the hypothesis, based on the finite element small scale yielding results, that the tensile near-tip asymptotic solution holds for a finite range of values of the remotely prescribed elastic phase angle, it is natural (see BPC) to prescribe a standard crack growth criterion (Rice, 1982), requiring that the crack propagate with an invariant near-tip crack opening profile. Equivalently, the crack growth criterion may be expressed as the restriction that the crack propagate with a constant plastic stress intensity factor, or

$$K_{pl} = K_c, \tag{24}$$

where K_c is a material parameter that would need to be determined experimentally.

Referring to relation (23), and observing that κ, as determined by the solution of the small scale yielding problem, is a function of the phase angle ψ, it can be concluded that there is a functional relation between the steady-state value of the applied elastic stress intensity factor K_{el} and the phase angle ψ, namely,

$$K_{el} = (\tau_0^{(2)})^{(2s+1)/2s}(\kappa(\psi)/K_c)^{1/2s}. \tag{25}$$

Relation (25) serves to identify a ductile mechanism explaining the widely reported experimental observation of a strong dependence of interfacial toughness on phase angle. In the next sub-section the predictions for interfacial toughness, as a function of the remote mode-mix, are reported.

4.2. *Results for interfacial toughness*

Figure 12(a)–(b) show two sets of results for the interfacial toughness. Each figure contains three different plots which are based on values of K_{pl} obtained from three different choices for the functions B_{ij} in relations (18)–(19). Thus, Fig. 12(a) shows results for cases where K_{pl} has been estimated from the functions B_{xx} at $\theta = 90^\circ$, D_{xx} at $\theta = 135^\circ$, and D_{yy} at $\theta = 135^\circ$, respectively, where D_{xx} and D_{yy} share the same definitions as B_{xx} and B_{yy} in relation (18), but with the stress component σ_{xx} and σ_{yy} replaced with the corresponding stress-deviator components s_{xx} and s_{yy},

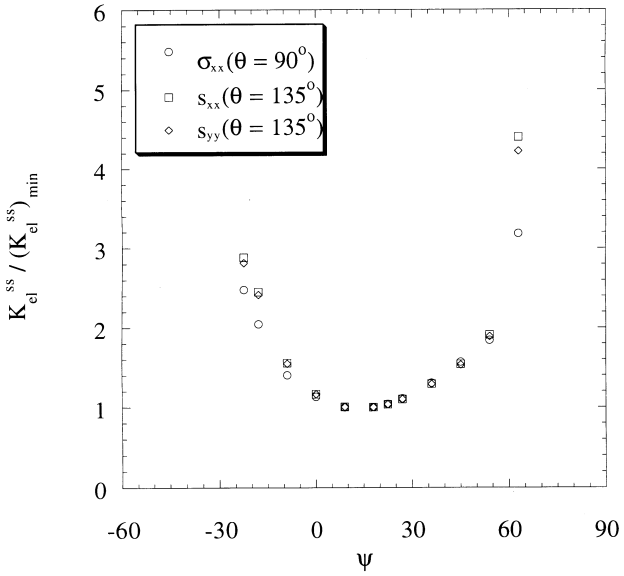

Fig. 12a. Interfacial toughness (K_{el}) as a function of the applied mode mix ψ. The different curves correspond to estimates for the plastic stress intensity factor obtained from σ_{xx} at $\theta = 90^\circ$, and s_{yy} and s_{xx}, respectively, at $\theta = 135^\circ$.

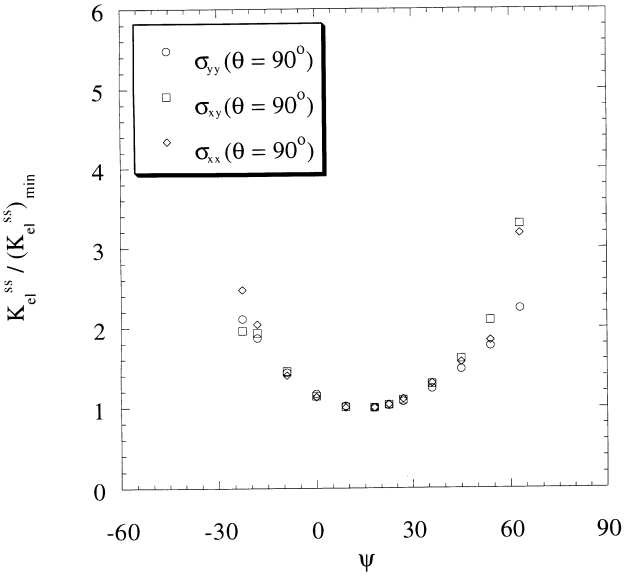

Fig. 12b. Interfacial toughness (K_{el}) as a function of the applied mode mix ψ. The different curves correspond to estimates for the plastic stress intensity factor obtained from σ_{yy}, σ_{xx} and σ_{xy}, respectively, at $\theta = 90^\circ$.

respectively. Each plot shows the interfacial toughness, as measured by K_{el} normalized by its minimum value $(K_{el})_{\min}$, as a function of ψ. Note that each plot has a common minimum value of 1, and this is a consequence of the normalization with respect to $(K_{el})_{\min}$ which is evaluated

separately for each case (the actual minimum values for the three cases are different to the extent the numerical estimates for K_{pl} are different). The toughness plots have the U-shape that has been observed experimentally, yielding toughness increases of up to factors of five or even higher for the steeper portions of the curves, for relatively small changes in the applied mode mix ψ. Also, the minimum of these plots lie in the positive shear range, and all the curves have some degree of asymmetry about their minimum points, with a steeper behavior in the direction of negative applied shear. These observations have the following consequences. The U-shapes imply that the interfacial toughness is a strong function of the applied mode mix ψ. The position of the minimum (in the positive shear range) suggests that the most favorable loading for continued steady propagation of the crack is probably not pure tension, but some combination of tension and shear. The asymmetry of the curves about their respective minimum points suggest that the resistance for continued propagation increases faster for applied negative shear than it does for applied positive shear. The latter behavior is not surprising given that the crack is propagating along a brittle/ductile interface, where it is reasonable to expect positive shear to tend to open up the crack, and negative shear to tend to shut it. Note that all the curves in Fig. 12(a) appear to share a common minimum position on the ψ-axis, which is close to $\psi = 15^\circ$. Also, all three plots are close to one another for a fairly wide range of values of ψ about the minimum point.

Figure 12(b) shows another set of three plots for the interfacial toughness. The results are based on K_{pl} evaluated from the functions B_{yy}, B_{xy}, and B_{xx}, respectively, at $\theta = 90^\circ$. All of the three plots are close to one another in the vicinity of their common minimum which, just like in Fig. 12(a), also appears to be approximately at $\psi = 15^\circ$. Outside of this range, for applied positive shear the results based on B_{xy} appears to be underestimating the toughness enhancement over its minimum value. However, for negative applied negative shear, the predictions from the three different sources appear to be fairly close to one another.

The results presented in this section identifies the role of plasticity in determining the interfacial toughness as a function of the applied mode mix. The predictions for interfacial toughness based on the asymptotic results and the full-field finite element results of the small scale yielding problem, are in good qualitative agreement with available experimental results.

Finally, we note that TH have also recently proposed a model to predict theoretically the influence of the remotely applied mode mix on interfacial toughness. Their model involves a local fracture criterion, which not only accounts for the plastic dissipation in the ductile phase, but additionally incorporates the effect of the fracture processes on the total energy balance. This is accomplished by attributing a constitutive law (Needleman, 1987) to the interface, as already explored by these authors in their investigation of crack propagation in homogeneous ductile solids (Tvergaard and Hutchinson, 1992). In addition, their model is capable of predicting the full resistance curve behavior of the propagating crack. In this paper only steady-state propagation was considered. Thus, the present work is complementary to the work of TH, and should correspond, in some sense, to the strong-interface limit of their steady-state results. To be more precise, it is suggestive that the toughening curves predicted in this work are similar in character to the "strong" tensile-interface (large $\hat{\sigma}/\sigma_Y$ and δ_n^c/δ_t^c) toughness-curve predictions of TH (see Fig. 8(b) in that reference). This is in spite of significant differences in the modeling of the problem, including a fracture process zone in the work of TH vs none here, power-hardening in TH vs linear-hardening here, and compressible behavior for the ductile material in TH vs incompressible behavior here. All of this appears to single out ductility as the main mechanism accounting for the mixed-mode toughening effect.

5. Concluding remarks

The aim of this work has been to validate the results of an earlier asymptotic analysis of steady quasi-static crack growth along a brittle–ductile interface under plane strain conditions, and also to assess the physical relevance of the asymptotic results. To this end, the small scale yielding (abbreviated SSY in the rest of this section) problem is solved using the finite element method, and the results compared with those obtained previously from the asymptotic analysis. It is observed that close to the crack tip the results of the SSY problem are consistent with the predictions of the asymptotic analysis. In particular, the SSY results confirm that the near-tip mode mix is, to a large extent, independent of the mode mix of the applied elastic fields for significantly wide ranges of the applied mode mix; and that in such cases, the near-tip fields feel the effect of the far-field only through the plastic stress intensity factor. Moreover, the results of the SSY problem suggest that out of the four possible near-tip states predicted by the asymptotic analysis—either the "tensile", or the "compressive" near-tip state will be preferred for most values of the remote mode mix. The "positive-shear" and the "negative-shear" near-tip states act more like unstable transitory states between the more stable "tensile" and "compressive" near-tip states. The corresponding results are significantly different in the absence of plasticity. In the latter case, the near-tip mode mix is not only strongly dependent on the applied elastic mode mix, but also varies continuously with it. The regions of validity of the asymptotic fields are estimated from the SSY results. It is observed that the regions of validity of the near-tip state are strong functions of the applied elastic mode mix. In addition, certain observations based on the micromechanics of ductile fracture suggest that the regions of validities of the asymptotic tensile fields may be significant fractions of the plastic zone size. This justifies the use of information obtained from the results of the asymptotic analysis to make global predictions on the behavior of an interfacial crack—such as the dependence of interfacial toughness on the applied elastic mode mix.

The work also explores a ductile mechanism to explain the strong dependence of interfacial toughness on applied mode mix during steady crack growth along strong interfaces between generally distinct elastoplastic phases. The results suggest that ductility plays an important role in the understanding of this phenomenon. Application of a standard crack growth criterion to a sequence of small scale yielding problems with varying mixed-mode conditions predicts U-shaped toughness-vs-phase angle curves. Although the effect of varying the hardening parameter has not been explored in the present work, it is expected that the U-shape effect will be enhanced by decreasing the hardening of the ductile phases (see Bose and Ponte Castañeda, 1995). Differences in the properties of the materials adjacent to the interface lead to asymmetry in the toughness curves. In particular, mixed-mode loadings with a finite positive-shear component, superimposed on a larger tensile component, actually appears to enhance crack growth, whereas negative shear has the opposite effect. This is consistent with what can be physically or intuitively expected for crack growth along the interface between a ductile and a brittle solid—namely that, positive shear should tend to open up the crack, while negative shear should tend to shut it. Connections have been made between the toughening curves predicted in this work vs the "strong" tensile-interface (large $\hat{\sigma}/\sigma_Y$ and δ_n^c/δ_t^c) toughness-curve predictions of TH. It appears that in spite of significant differences in the modeling of the problem, the final results of TH and the present work are similar in essence.

Finally, it may be noted that, although linear-hardening does not model the uniaxial stress–

strain response of most metals, its application to the present class of problems can be amply justified. The reader is referred to BPC for further discussion on this aspect of the problem. It should also be noted however that, some preliminary finite-element results for the full field problem of steady quasi-static crack growth along the interface between a rigid material and a power-law hardening ductile solid indicates that the values of mode-mix in the vicinity of the crack tip are discrete and independent of the applied elastic mode mix.

Acknowledgements

This work was supported by the National Science Foundation/Materials Research Laboratory Program at the University of Pennsylvania under Grant No. DMR91-20668.

References

Anderson, G. P., De Vries, K. L. and Williams, M. L. (1974) The influence of loading direction upon the character of adhesive bonding. *J. Colloid and Int. Sci.* **47,** 600–609.

Bose, K. (1995) Steady interfacial crack growth under mixed-mode conditions. Ph.D. dissertation, Department of Mechanical Engineering and Applied Mechanics, University of Pennsylvania.

Bose, K. and Ponte Castañeda, P. (1992) Stable crack growth under mixed mode conditions. *Journal of the Mechanics and Physics of Solids* **40,** 1053–1103.

Bose, K. and Ponte Castañeda, P. (1995) The effect of mode mix on interfacial toughness: a ductile mechanism. *Fracture Mechanics*: 25*th Volume*, *ASTM STP*, ed. F. Erdogan, **1220,** 106–124. American Society of Testing and Materials, Philadelphia.

Cao, H. C. and Evans, A. G. (1989) An experimental study of the fracture resistance of bimaterial interfaces. *Mech. of Mater.* **7,** 295–304.

Dean, R. H. and Hutchinson, J. W. (1980) Quasi-state steady crack growth in small-scale yielding. *Fracture Mechanics*: *Twelfth Conference*, *ASTM STP*, **700,** 383–405. American Society for Testing and Materials.

Deng, X. and Rosakis, A. J. (1992) A finite-element investigation of quasi-static and asymptotic crack-tip fields in hardening elastic–plastic solids under plane stress. Part I: Crack growth in linear hardening materials. *International Journal of Fracture* **57,** 291–308.

Evans, A. G. and Hutchinson, J. W. (1989) Effect of non-planarity on the mixed-mode fracture resistance of bimaterial interfaces. *Acta Metallica* **37,** 909–916.

Hutchinson, J. W. (1968) Singular behavior at the end of a tensile crack in a hardening material. *Journal of the Mechanics and Physics of Solids* **16,** 13–31.

Hutchinson, J. W. and Suo, Z. (1991) Mixed mode cracking in layered materials. *Advances in Applied Mechanics* **29,** 63–191.

Liechti, K. M. and Chai, Y. S. (1991) Biaxial loading experiments for determining interfacial toughness. *Journal of Applied Mechanics* **58,** 680–687.

Liechti, K. M. and Chai, Y. S. (1992) Asymmetric shielding in interfacial fracture under in-plane shear. *Journal of Applied Mechanics* **59,** 295–304.

Liechti, K. M. and Hanson, E. C. (1988) Nonlinear effects in mixed-mode interfacial delaminations. *International Journal of Fracture* **36,** 195–217.

Mataga, P. A. (1986) High strain-rate crack growth. Ph.D. dissertation, Division of Applied Sciences, Harvard University.

Mataga, P. A. (1989) Unpublished work.

McClintock, F. A. and Argon, A. S. (1966) *Mechanical Behavior of Materials*. Addison-Wesley Publishing Company.

Needleman, A. (1987) A continuum model for void nucleation by inclusion debonding. *Journal of Applied Mechanics* **54,** 525–531.

O'Dowd, N. P. and Shih, C. F. (1991) A family of crack tip fields characterized by a triaxiality parameter: Part I—Structure of fields. *Journal of the Mechanics and Physics of Solids* **39,** 989–1015.

O'Dowd, N. P. and Shih, C. F. (1992) A family of crack tip fields characterized by a triaxiality parameter: Part II—Fracture applications. *Journal of the Mechanics and Physics of Solids* **40,** 939–963.

Omprakash, S. and Narasimhan, R. (1996) A finite element analysis of mode III quasi-static crack growth at a ductile–brittle interface. *Journal of Applied Mechanics* **63,** 204–209.

Ponte Castañeda, P. and Mataga, P. A. (1991) Stable crack growth along a brittle/ductile interface—I. Near-tip fields. *International Journal of Solids and Structures* **27,** 105–133.

Ranjith, K. and Narasimhan, R. (1996) Asymptotic and finite element analysis of mode III dynamic crack growth at a ductile–brittle interface. *International Journal of Fracture* **76,** 61–77.

Rice, J. R. and Rosengren, G. F. (1968) Plane strain deformation near a crack tip in a power-law hardening material. *Journal of the Mechanics and Physics of Solids* **16,** 1–12.

Rice, J. R. (1982) Elastic plastic crack growth. *Mechanics of Solids*: *The Rodney Hill* 60*th Anniversary Volume*, ed. H. G. Hopkins and M. J. Sewell, pp. 539–562. Pergamon Press, Oxford.

Sharma, S. M. and Aravas, N. (1993) On the development of variable–separable asymptotic elastoplastic solutions for interfacial cracks. *International Journal of Solids and Structures* **30,** 695–723.

Sharma, S. M., Aravas, N. and Zelman, M. G. (1995) Two-parameter characterization of crack tip fields in edge-cracked geometries: plasticity and creep solutions. *Fracture Mechanics*: 25*th Volume*, *ASTM STP*, ed. F. Erdogan, **1220,** 309–327. American Society for Testing and Materials, Philadelphia, pp. 309–327.

Shih, C. F. (1974) Small-scale yielding analysis of mixed mode plane-strain crack problems. *Fracture Analysis*, *ASTM STP* **560,** 187–210. American Society of Testing and Materials.

Trantina, G. C. (1972) Combined mode crack extension in adhesive joints. *J. Comp. Mater*. **6,** 271–385.

Tvergaard, V. and Hutchinson, J. W. (1992) The relation between crack growth resistance and fracture process parameters in elastic–plastic solids. *Journal of the Mechanics and Physics of Solids* **40,** 1377–1397.

Tvergaard, V. and Hutchinson, J. W. (1993) The influence of plasticity on mixed mode interface toughness. *Journal of the Mechanics and Physics of Solids* **41,** 1119–1135.

Varias, A. G. and Shih, C. F. (1993) Quasi-static crack advance under a range of constraints—steady-state fields based on a characteristic length. *Journal of the Mechanics and Physics of Solids* **41,** 835–861.

Wang, J.-S. and Suo, Z. (1990) Experimental determination of interfacial toughness curves using brazil-nut sandwiches. *Acta Metallica Materiala* **38,** 1279–1290.

Williams, M. L. (1959) The stresses around a fault or crack in dissimilar media. *Bull. Seismm. Soc. Am*. **49,** 199–204.